Beta-adrenergic agonists alter glucose and mitochondrial metabolite utilization independent of a fiber type shift

by

Sidney Anne Munk

B.S., Virginia Tech, 2022

A THESIS

submitted in partial fulfillment of the requirements for the degree

MASTER OF SCIENCE

Department of Animal Sciences and Industry
College of Agriculture

KANSAS STATE UNIVERSITY
Manhattan, Kansas

2025

Approved by:

Major Professor
Morgan Daughtry Zumbaugh

Copyright

Abstract

A growing population with diminishing agricultural inputs calls for the livestock industry to incorporate strategies for greater production efficiency. Understanding the biochemical pathways that skeletal muscle utilizes to metabolize nutrients in livestock species can aid in this effort. To investigate changes that occur as the metabolic profile of skeletal muscle shifts, we supplemented pigs with the beta-adrenergic agonist ractopamine hydrochloride (BAA). This pharmacological agent provides an ideal model to induce a metabolic shift without altering genetics, nutrition, or management strategy. Therefore, the objective of this study was to define the BAA-mediated metabolic response in skeletal muscle with inherently different metabolic profiles through assessing changes in myosin heavy chain (MyHC) isoforms, metabolic enzymes, and metabolite utilization. Mature DNA 600 x 241 barrows (DNA Genetics) were fed a standard commercial diet containing 16% crude protein supplemented with 0 g/ton (control; n = 8) or 9 g/ton ractopamine hydrochloride (BAA; n = 10) for 2 weeks. Samples were collected from the *longissimus dorsi* (LD, glycolytic muscle), *latissimus dorsi* (LAT, mixed muscle), *semitendinosus* (ST, mixed muscle), and *masseter* (MS, oxidative muscle). To determine if BAA feeding induced changes in fiber type, MyHC isoforms were measured because this approach is the traditional method of muscle fiber type classification. Although there were muscle differences in MYH7, MYH2, MYH1, and MYH4 isoforms (muscle; $p < 0.05$), there were no treatment differences ($p > 0.05$). The half-life of myosin is approximately the duration of BAA feeding, which may partially explain the lack of BAA induced changes in MyHC isoforms. Therefore, we evaluated glycolytic and oxidative enzymes to assess metabolic adaptations that may occur without altering MyHC isoforms present. While there were differences in PFK activity, LDHα protein abundance, or SDHα protein abundance between muscles evaluated ($p < 0.05$), there were no treatment

differences ($p > 0.05$). However, abundance of PC decreased in all BAA muscles compared to control muscles ($p < 0.05$), which suggests BAA feeding may diminish oxidation of the glycolytic end product pyruvate. To investigate changes in glycolytic flux, concentrations of glucose, G6P, and lactate were measured. In addition to differences in these glycolytic intermediates across muscles, glucose and G6P decreased in all BAA muscles compared to control muscles ($p < 0.05$). However, lactate concentration did not differ between BAA and control muscles suggesting BAA feeding prioritizes the utilization of diminished glycolytic intermediates in the Cori cycle. To determine if BAA mitochondria decrease pyruvate oxidation, isolated mitochondria were incubated with [$^{13}C_3$]-pyruvate. These data indicate changes in the amount of an isotopomer derived from pyruvate rather than the total amount of an intermediate present. Isotopic enrichment of oxaloacetate (OAA) M + 2 increased in BAA LAT mitochondria compared to control LAT ($p < 0.05$). In addition, OAA M + 2 increased in BAA LAT mitochondria compared to control and BAA MS mitochondria (muscle * treatment; $p < 0.05$). In addition, citrate M + 2, M + 3, M + 4, and α-ketoglutarate M + 4 and M + 5 enrichment decreased in BAA LAT mitochondria compared to all other mitochondria ($p < 0.05$). Further, citrate M + 6 and α-ketoglutarate M + 2 and M + 3 enrichment decreased in BAA mitochondria ($p < 0.05$). Collectively, these data demonstrate BAA supplementation induced changes in glucose utilization independent of frequently measured indicators of metabolic shifts.

Table of Contents

List of Figures

List of Tables

Acknowledgements

First and foremost, I want to thank my major advisor, Dr. Morgan Zumbaugh, for being my mentor over the last two years. I never expected to get a degree in meat science, but thankfully you are very persuasive. Somehow you knew that I would love this work, and I will be forever grateful that you convinced me to stay in Kansas for a couple more years, because it is the best decision I have ever made. The knowledge that I have gained under your guidance is invaluable. Words cannot express my thanks and gratitude for you.

Secondly, I want to thank Linnea Rimmer for the guidance you have given me. I truly don't think I could have done this without you. Thank you for always taking the time to teach me about everything we do, relating to my problems, for laughing and crying with me, and always having a shoulder for me to lean on, even when you had a million other better things to do. Finding a friend in you has truly been such a blessing and I cannot thank you enough for all the time and friendship you have given me.

To my committee members, Dr. Travis O'Quinn and Dr. Michael Chao, thank you for all your guidance and mentorship. To Travis, thank you for teaching me about all things meat and for being patient when trying to explain statistics to me. To Dr. Chao, thank you for the time you have spent with me in the lab, even just in passing, to discuss different assays, and for teaching me about the more technical aspects of our subject matter. I have really enjoyed our time together and am so grateful to you both.

As for the rest of the meat science faculty, I would like to thank Dr. Jessie Vipham for also being a mentor to me. You were always encouraging if I was in a tough spot and reminded me to look at the bigger, brighter picture. To Dr. Erin Beyer, thank you for always being willing to help me out or talk something through, and for being a friend. I have enjoyed getting to know you this

past year. You are both wonderful teachers and have taught me so much, and I will always be grateful for that.

To the meat science graduate students, you all have made these past two years some of the most fun I have ever had, even if they were some of the most stressful. I especially want to thank Lauren, Ashton, Greta, Chesney, and Steph, as you have all been such wonderful friends to me. Between bonding over cooking for panels, helping me out in the lab, pet sitting, going to sporting events together, and much more, I have had so much fun getting to know you all and am so lucky to have a friend in each one of you. To the other grad students, I have had so much fun getting to know you all have enjoyed our time together.

While I could just as easily group Mason in with the other grad kids I shouted out, I suppose you've earned a little section to yourself. Thank you for all you have taught me, both in and out of school. You have been a light in my life practically since day one here. You've been an amazing friend and companion and have been so grounding throughout these years. Thank you for giving me a home here in Kansas. I'm so lucky to have been able to go through this experience with you and look forward to whatever's next.

To my family, Mom, Dad, Casey, and Emma, thank you for being the strongest supporters I know. I would not have had the courage to do half of the things that I have done in my life if not for your continual support and advise and love. No number of words can express the gratitude and love I have for you all. I love you so much.

Chapter 1 - Literature Review

Introduction

The global population is projected to reach approximately 8.4 billion people by 2031 (Dohlman et al., 2022), increasing the number of people to feed but diminishing land available for food production. In addition, meat consumption is at an all-time high (Cawthorn and Hoffman, 2014). These growing constraints call for continued advancements to improve meat animal production efficiency within the limitations of less land and fewer resources. To date, the livestock industry has developed and implemented advancements to increase meat production with fewer agricultural inputs, largely through improvements in genetic selection, nutrition, management, and feed additives. For example, in the past 33 years, there has been a 17% increase in carcass weight with a 4% decrease in feed consumption (Tokach et al., 2016). While these strategies are essential for sustained progress, additional innovation to continue advancing production efficiency is necessary to accommodate future demands with less land and resource availability. Understanding the underlying physiology of how nutrients from feed are converted into tissue will aid in advancing practices to improve feed efficiency.

Skeletal muscle is the largest tissue in the body that accounts for the majority of global glucose consumption (Ferrannini et al., 1988). Therefore, changes in skeletal muscle metabolism and nutrient utilization impact whole body metabolism and performance (Gunawan et al., 2020). For example, the two major metabolic pathways that fuel skeletal muscle function and growth are glycolysis and oxidative phosphorylation. While glycolysis generates a net yield of two molecules of ATP and oxidative phosphorylation can generate up to 32 ATP molecules, glycolysis converts glucose into two molecules of pyruvate and can conserve carbon backbones for anabolic processes. The cellular preservation of carbon and efficiency of glycolysis is best illustrated by metabolism

of many types of cancer, where the Warburg Effect facilitates glycolytic metabolites to enter anabolic pathways while producing ATP to support cellular function (Kukurugya et al., 2024). During oxidative phosphorylation, ATP is produced along with heat, CO_2, and water, resulting in a loss of carbon rendering the process less efficient in regard to livestock growth. In fact, muscle of animals that exhibit improved feed efficiency upregulate glycolytic metabolism and suppress oxidative enzymes (Fu et al., 2017). However, the mechanisms that dictate efficient nutrient utilization in skeletal muscle remain vague.

Metabolism is typically characterized by measuring parameters such as protein abundance, gene expression, metabolite concentration, and enzyme activity. For example, evaluating pyruvate dehydrogenase alpha (PDHα) is an indicator of oxidative capacity due to its role as one of the entry points of pyruvate in the tricarboxylic acid (TCA) cycle. However, the multiple layers of regulation that regulate PDH complex activity make it difficult to account for minor alterations in the utilization of metabolites within a system. For example, while greater PDHα protein abundance may suggest an increase in pyruvate conversion to acetyl-CoA, post-translational modifications alter its activity. Further, this methodology alone may not reveal alterations to pyruvate utilization in the TCA cycle. While much work has been done to establish methodology to characterize muscle as predominately glycolytic or oxidative in nature, additional research is necessary to understand how different muscles utilize nutrients. In particular, muscles classified as mixed or intermediate have been understudied while those classified as highly glycolytic or oxidative muscles are often evaluated.

To begin to understand how metabolites are utilized in different muscles and identify mechanisms that facilitate changes in metabolite utilization, feeding beta-adrenergic agonists (BAA) provides a model to use the same genetics, feeding regiment, age, sex, rearing, handling,

and environmental conditions to initiate a metabolic shift. These pharmacological agents have been used in the agricultural industry to promote feed efficiency of various species, including turkeys, cattle, and swine. Ractopamine hydrochloride, a type of BAA, has been widely studied and characterized to improve growth performance and feed efficiency in swine as well as promote a fiber-type shift in skeletal muscle (Watkins et al., 1990; Carr et al., 2005; Panisson et al., 2020). While ractopamine improves growth performance, conditions of feeding and breed type influence the degree of improvement. For example, Mangalica pigs, known for producing carcasses with high fat deposition, exhibited a 24% increase in average daily gain (ADG) after 3 weeks of ractopamine supplementation, while pigs harboring genetics more similar to commercial pigs had a 20% increase in ADG after six weeks of ractopamine supplementation (Soares et al., 2022; Reeves Pitts et al., 2023). Further, ractopamine induces a metabolic shift towards more glycolytic muscles under certain feeding conditions, which may contribute to improved production efficiency (Gunawan et al., 2007). However, the mechanisms that drive this shift remain undefined. Therefore, the objective of this literature review is to give an overview of skeletal muscle metabolism, the classification of muscle fibers and their metabolic profile, and the use of ractopamine as a model to investigate the regulation of skeletal muscle metabolism.

Overview of skeletal muscle metabolism

Glycolysis

Glycolysis converts glucose to pyruvate through a ten-step enzymatic process producing a net of 2 ATP, 2 NADH, 2 H^+, and H_2O in the sarcoplasm of muscle cells. After feedings, muscle takes up glucose through glucose transporter type 4 (GLUT4) and hexokinase then converts glucose to glucose-6-phosphate (G6P) in the first step of glycolysis (Richter and Hargreaves, 2013). During states of low glucose, such as those between feedings, glycogen phosphorylase breaks down glycogen into glucose-1-phosphate, which can be converted to G6P. Depending on

cellular needs, G6P can enter the pentose phosphate pathway (PPP) to produce 5-carbon precursors for biosynthetic processes or continue through glycolysis to produce pyruvate. Glucose 6-phosphate dehydrogenase (G6PDH) converts G6P to 6-phosphogluconolactone in the first step of the oxidative branch of the PPP to produce ribose-5-phosphate for nucleotide synthesis and nicotinamide adenine dinucleotide phosphate (NADPH) for amino acid and nucleotide synthesis. In addition, G6P can be diverted to the PPP during periods of high oxidative stress and times of greater cellular need for NADPH, which depicts the importance of this pathway in supporting cellular processes (Riganti et al., 2012). Although muscle is post-mitotic, and thus does not require 5-carbon precursors for DNA synthesis, the PPP is employed by muscle during hypertrophy, presumably for RNA synthesis or to combat oxidative stress (Rajas et al., 2019; Valentino et al., 2021). Alternatively, G6P can continue through glycolysis in a series of stepwise enzymatic reactions.

While majority of glycolytic intermediates will be metabolized to produce pyruvate, other ancillary pathways branch from glycolysis to support anabolism in muscle (Villee et al., 1952). For example, the glycolytic intermediate 3-phosphoglycerate (3-PG) can enter the serine biosynthesis pathway through phosphoglycerate dehydrogenase (PHGDH) and subsequently generate serine, which is a precursor to lipids, amino acids, and nucleotides (Yamasaki et al., 2001). The glycolytic end product, pyruvate, also has multiple fates. Lactate dehydrogenase alpha (LDHα) converts pyruvate to lactate, which can be exported from muscle cells for transport to the liver to replenish glucose stores through gluconeogenesis. This process is termed the Cori Cycle and is often employed by glycolytic muscle to enable continued glycolytic flux. Conversely, pyruvate can enter the tricarboxylic acid (TCA) cycle through pyruvate dehydrogenase (PDH) or

pyruvate carboxylase (PC). Glycolysis provides many of the fundamental intermediates necessary for biosynthetic processes.

TCA Cycle

In the mitochondrial matrix, TCA cycle enzymes metabolize intermediates of carbohydrate, lipid, and amino acid metabolism. The TCA cycle is not a carbon sink, and therefore, a continual efflux and influx of TCA intermediates occurs. Intermediates are replenished through anaplerosis and depleted through cataplerosis (Owen et al., 2002). For example, glutamic-oxaloacetic transaminase 2 (GOT2) catalyzes the conversion of oxaloacetate to aspartate in a cataplerotic reaction to remove oxaloacetate from the TCA cycle. Similarly, glutamate dehydrogenase (GDH) converts α-ketoglutarate to glutamate for use in other metabolic processes. Conversely, GDH can catalyze its intermediates in both directions, and therefore can also facilitate anaplerosis through the conversion of glutamate to α-ketoglutarate. Many enzymes supply and consume TCA cycle intermediates to support the dynamic needs of myofibers.

Pyruvate, the glycolytic end product, is transported into the mitochondrial matrix and can enter the TCA cycle through PDH or PC. Pyruvate is largely converted to acetyl-CoA through PDH, which also yields CO_2, NADH, and H^+. Alternatively, a small portion of pyruvate is converted to oxaloacetate by PC while also consuming a bicarbonate molecule. Both of these anaplerotic enzymes facilitate entry of intermediates of carbohydrate metabolism into the TCA cycle, although PC-mediated entry conserves carbon backbones whereas PDH-mediate entry losses carbon as exhaled CO_2. Regardless of entry point, these intermediates can proceed through the TCA cycle to generate reducing equivalents for ATP synthesis in the electron transport chain (ETC) or exit the cycle through cataplerotic reactions to support alternative biochemical processes.

Amino acid metabolism can fuel the TCA cycle during periods of diminished feed intake or under atrophic conditions as well as support transamination and deamination of different amino acids. For example, pyruvate-derived intermediates can exit the TCA cycle through cataplerotic reactions to produce amino acids, such as GDH converting α-ketoglutarate to glutamate. Further, dietary amino acids can enter and exit the TCA cycle to generate different amino acids through transamination and deamination (Figure 1.1), such as GDH converting glutamate to α-ketoglutarate to produce oxaloacetate for GOT2 to convert to aspartate. Conversely, amino acids can fuel the TCA cycle during periods of low energy demands. Fatty acids also feed into the TCA cycle after undergoing beta-oxidation to produce acetyl-CoA. Beta-oxidation catabolizes fatty acids in the mitochondrial matrix to supply the TCA cycle with acetyl-CoA, which can be used to generate reducing equivalents or exit the cycle through cataplerosis. Continual cataplerosis and anaplerosis of metabolites occur to support the dynamics needs of postnatal muscle growth.

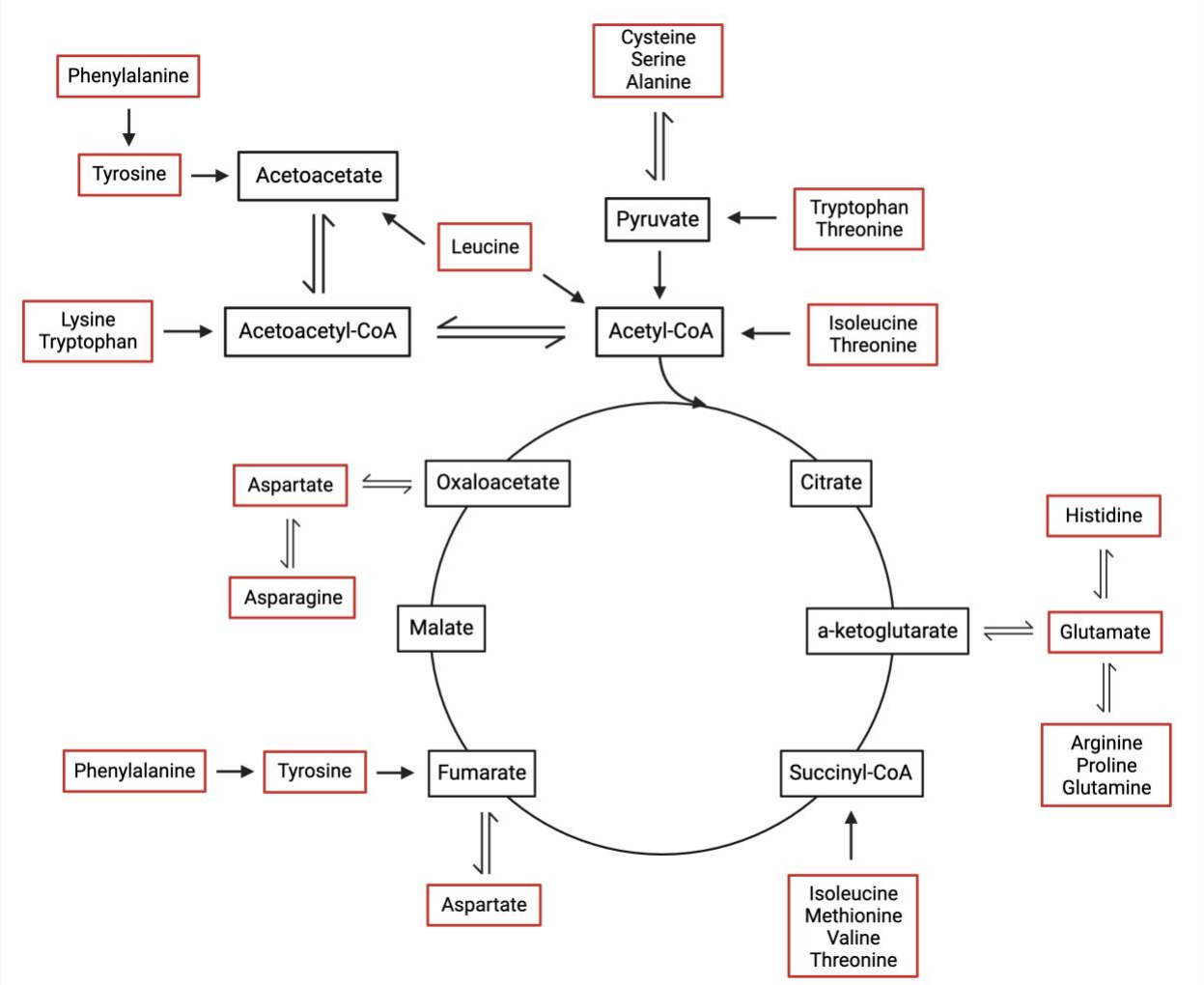

Figure 1.1. The contribution of amino acids from the TCA cycle. Amino acids are displayed in red boxes. Arrows depict the direction of the enzymatic reaction.

Energy in the form of ATP is generated through ETC-mediated oxidation of reducing equivalents produced in the TCA cycle. Briefly, complex I and II respectively oxidize NADH and $FADH_2$ to facilitate electron transfer to complex III and subsequently complex IV. During this process of electron transfer, complexes I, III, and IV pump H^+ ions from the mitochondrial matrix to the inner membrane space generating the mitochondrial membrane potential. Complex V, also known as ATP synthase, harnesses this electrochemical gradient to produce ATP as H^+ re-enters

the matrix. Approximately 32 molecules of ATP are produced per molecule of glucose (Deshpande and Mohiuddin, 2024). Oxidized NAD^+ and FADH molecules are then reduced in glycolysis or the TCA cycle to continue powering the ETC.

Muscle fiber plasticity and classification of muscle fibers

Skeletal muscle is a heterogenous tissue comprised of muscle fibers that can generally be classified by fiber type, which is determined by speed of contraction and metabolic characteristics. Type I fibers exhibit a slower rate of ATP hydrolysis and twitch mechanism than type II fibers (He et al., 2000). Therefore, type I fibers are classified as slow and type II as fast fibers. In addition, type I fibers largely rely on oxidative phosphorylation to produce ATP. As a result, these fibers have high amounts of mitochondria and fatigue at a slower rate than glycolytic fibers. Type II fibers have three classifications: IIa, IIx, and IIb (Schiaffino et al., 1989). While all type II fibers are characterized as fast twitch, the subtypes range in metabolic characteristics, with IIa having a higher oxidative capacity and IIx and IIb being more glycolytic (Larsson et al., 1991). Given muscles are made up of a heterogeneous population of muscle fibers, the overall metabolic classification of a muscle is the result of fiber type composition within each muscle (Sano et al., 2007). Metabolism can also vary across a muscle, which is often observed in muscles that span from a deep to superficial anatomical region. For example, *semitendinosus* (ST) muscles have more type I and IIa fibers in the deep portion and IIx and IIb fibers in the superficial portion of the muscle giving rise to a gradient across the muscle (Larsson et al., 1991).

Although location in the body is a major determinant of skeletal muscle metabolism, the overall metabolic profile of muscles are influenced by intrinsic and extrinsic factors, such as nutrition, genetics, use, and stress (Park et al., 2009; Muroya, 2023). For example, muscle from grass-fed cattle exhibit higher amounts of oxidative enzymes and fewer glycolytic enzymes

compared to grain-fed cattle (Apaoblaza et al., 2020). Further, upregulation of peroxisome proliferator-activated receptor gamma coactivator (PGC1α), a transcription factor that promotes mitochondrial biogenesis, increased mitochondrial content and levels of myoglobin resulting in greater oxidative capacity and number of type I fibers in the *gastrocnemius* muscle (Zhang et al., 2017). Given skeletal muscle is responsive to stimuli, understanding factors that influence the metabolic characteristics of myofibers has potential to impact nutrient utilization during growth as well as meat quality characteristics after slaughter.

To study skeletal muscle metabolism, methodologies to characterize metabolic changes have been established. Histochemical techniques involving myosin ATPase staining as well as evaluation of myosin heavy chains (MyHC) have been established as routine methodology to classify muscle fibers (Gunawan et al., 2007; Eggers et al., 2021). Isoforms of MyHC are often assessed through measuring gene expression, protein abundance, or histochemistry to classify fibers. Type I, IIa, IIx, and IIb fibers express MYH7, MYH2, MYH1, and MYH4 genes, respectively (Schiaffino and Reggiani, 2011; Eggers et al., 2021). Given muscle is a heterogenous population of muscle fibers, histochemical analysis permits quantification of fiber type distribution whereas other methods of detection are a cumulative measurement of fibers within the muscle (Peter et al., 1972; Lowry et al., 1978).While MyHC isoforms are often used to classify fibers, the protein turnover rate of myosin isoforms is a half-life of approximately 14.5 days but is dependent on different factors such as stimuli and age (Rolfs et al., 2021). Therefore, detecting subtle changes in metabolic characteristics may be overlooked when evaluating MyHC isoforms alone.

Because skeletal muscle metabolism is a complex process, it is essential to gather evidence through multiple avenues to define its metabolic profile. For example, the turnover rate of MyHC isoforms can mask underlying shifts in enzyme activity and metabolite utilization. Therefore, it is

important to include methodology that also evaluates metabolic characteristics in addition to MyHC when investigating skeletal muscle metabolism. While general conclusions can be drawn about the metabolic profile based on fiber type, evaluation of protein activity and abundance provides additional information. For example, type I fibers exhibit a high activity and abundance of oxidative enzymes, such as succinate dehydrogenase (SDH) (Essen et al., 1975; Schiaffino and Reggiani, 2011). Contrarily, type IIb fibers are classified as having a high activity of glycolytic enzymes, such as LDHα (Peter et al., 1972). In growing pigs, the *longissimus dorsi* (LD) has a higher abundance of LDHα and lower abundance of citrate synthase (CS) than the *masseter* (MS) from weaning to market, which are respectively glycolytic and oxidative muscles (Rimmer et al., 2024). While the enzymatic profile of highly oxidative and highly glycolytic muscle classifications are well defined and generally correspond to their metabolic classification based on fiber type, intermediate muscles such as the *latissimus dorsi* (LAT) are not as straightforward. For example, Rimmer et al. (2024) demonstrated the LAT exhibits high PC abundance similar to the MS, which is indicative of an oxidative phenotype. However, LDHα abundance was higher in the LAT and LD compared to the MS (Rimmer et al., 2024), which suggests intermediate muscles may rely on different aspects of these biochemical pathways to meet cellular energy demands. Further, Park et al. (2009) demonstrated differences in MyHC isoform abundance and gene expression in pigs harboring naturally occurring mutations, but no differences in gene expression of oxidative or glycolytic enzymes associated with the respective to MyHC type. Further, Gunawan et al. (2007) showed that swine fed ractopamine exhibited an increase in MyHC IIb expression throughout four weeks of feeding, but no differences in expression of LDHα were reported. This raises the question of if enzyme evaluation provides enough evidence to draw conclusions about metabolic shifts occurring within a short period. For example, while fiber type classifications are often used to infer

information about the metabolic profile of muscle, the complexity of metabolism calls for a more comprehensive assessment of the underlying biochemistry to understand nutrient utilization of skeletal muscle in livestock species.

Conclusion

The livestock industry has implemented many advancements such as improved nutrition and genetic selection to increase the amount of meat produced in the United States. However, the increasing population and growing number of meat consumers globally requires innovative approaches to secure further improvements in production efficiency to meet the growing demand. Understand the intricacies of skeletal muscle metabolism will aid in the efforts to meet these production goals. This literature review discusses the complexities of investigating and defining skeletal muscle metabolism, including potential pitfalls associated with different measures commonly used to classify muscle fiber type and general metabolic profile. To uncover approaches to improve nutrient utilization efficiency during muscle hypertrophy, a comprehensive assessment of metabolism should be utilized. For example, using multiple methodologies such as enzyme activity and abundance, MyHC isoform expression, and evaluation of metabolic intermediates are necessary to attempt to uncover the underlying biochemical processes in growing skeletal muscle. Further, these insights may uncover mechanisms that induce metabolic shifts. Collectively, skeletal muscle metabolism influences livestock production performance and exploring its biochemistry can aid in the effort to improve production efficiency.

References

Apaoblaza, A., S. D. Gerrard, S. K. Matarneh, J. C. Wicks, L. Kirkpatrick, E. M. England, T. L. Scheffler, S. K. Duckett, H. Shi, S. L. Silva, A. L. Grant, and D. E. Gerrard. 2020. Muscle from grass- and grain-fed cattle differs energetically. Meat Sci 161:107996. doi:10.1016/j.meatsci.2019.107996

Carr, S. N., D. J. Ivers, D. B. Anderson, D. J. Jones, D. H. Mowrey, M. B. England, J. Killefer, P. J. Rincker, and F. K. McKeith. 2005. The effects of ractopamine hydrochloride on lean carcass yields and pork quality characteristics. Journal of Animal Science 83:2886-2893. doi:10.2527/2005.83122886x

Cawthorn, D.-M., and L. C. Hoffman. 2014. The role of traditional and non-traditional meat animals in feeding a growing and evolving world. Animal Frontiers 4:6-12. doi:10.2527/af.2014-0027

Deshpande, O. A., and S. S. Mohiuddin. 2024. Biochemistry, Oxidative Phosphorylation. StatPearls, Treasure Island (FL).

Dohlman, E., J. Hansen, and D. Boussios. 2022. USDA Agricultural Projections to 2031.

Eggers, B., K. Schork, M. Turewicz, K. Barkovits, M. Eisenacher, R. Schroder, C. S. Clemen, and K. Marcus. 2021. Advanced Fiber Type-Specific Protein Profiles Derived from Adult Murine Skeletal Muscle. Proteomes 9. doi:10.3390/proteomes9020028

Essen, B., E. Jansson, J. Henriksson, A. W. Taylor, and B. Saltin. 1975. Metabolic characteristics of fibre types in human skeletal muscle. Acta Physiol Scand 95:153-165. doi:10.1111/j.1748-1716.1975.tb10038.x

Ferrannini, E., D. C. Simonson, L. D. Katz, G. Reichard, Jr., S. Bevilacqua, E. J. Barrett, M. Olsson, and R. A. DeFronzo. 1988. The disposal of an oral glucose load in patients with non-insulin-dependent diabetes. Metabolism 37:79-85. doi:10.1016/0026-0495(88)90033-9

Fu, L., Y. Xu, Y. Hou, X. Qi, L. Zhou, H. Liu, Y. Luan, L. Jing, Y. Miao, S. Zhao, H. Liu, and X. Li. 2017. Proteomic analysis indicates that mitochondrial energy metabolism in skeletal muscle tissue is negatively correlated with feed efficiency in pigs. Sci Rep 7:45291. doi:10.1038/srep45291

Gunawan, A. M., B. T. Richert, A. P. Schinckel, A. L. Grant, and D. E. Gerrard. 2007. Ractopamine induces differential gene expression in porcine skeletal muscles. J Anim Sci 85:2115-2124. doi:10.2527/jas.2006-540

Gunawan, A. M., C. N. Yen, B. T. Richert, A. P. Schinckel, A. L. Grant, and D. E. Gerrard. 2020. Ractopamine-induced fiber type-specific gene expression in porcine skeletal muscles is independent of growth. J Anim Sci 98. doi:10.1093/jas/skaa341

He, Z. H., R. Bottinelli, M. A. Pellegrino, M. A. Ferenczi, and C. Reggiani. 2000. ATP consumption and efficiency of human single muscle fibers with different myosin isoform composition. Biophys J 79:945-961. doi:10.1016/S0006-3495(00)76349-1

Kukurugya, M. A., S. Rosset, and D. V. Titov. 2024. The Warburg Effect is the result of faster ATP production by glycolysis than respiration. Proc Natl Acad Sci U S A 121:e2409509121. doi:10.1073/pnas.2409509121

Larsson, L., L. Edstrom, B. Lindegren, L. Gorza, and S. Schiaffino. 1991. MHC composition and enzyme-histochemical and physiological properties of a novel fast-twitch motor unit type. Am J Physiol 261:C93-101. doi:10.1152/ajpcell.1991.261.1.C93

Lowry, C. V., J. S. Kimmey, S. Felder, M. M. Chi, K. K. Kaiser, P. N. Passonneau, K. A. Kirk, and O. H. Lowry. 1978. Enzyme patterns in single human muscle fibers. J Biol Chem 253:8269-8277.

Muroya, S. 2023. An insight into farm animal skeletal muscle metabolism based on a metabolomics approach. Meat Sci 195. doi:10.1016/j.meatsci.2022.108995

Owen, O. E., S. C. Kalhan, and R. W. Hanson. 2002. The key role of anaplerosis and cataplerosis for citric acid cycle function. J Biol Chem 277:30409-30412. doi:10.1074/jbc.R200006200

Panisson, J. C., A. Maiorka, S. G. Oliveira, A. Saraiva, M. S. Duarte, K. F. Silva, E. V. Santos, R. L. S. Tolentino, I. M. G. Lopes, L. L. M. Guedes, and B. A. N. Silva. 2020. Effect of ractopamine and conjugated linoleic acid on performance of late finishing pigs. Animal Frontiers 14:277-284. doi:10.1017/S1751731119001708

Park, S. K., A. M. Gunawan, T. L. Scheffler, A. L. Grant, and D. E. Gerrard. 2009. Myosin heavy chain isoform content and energy metabolism can be uncoupled in pig skeletal muscle. J Anim Sci 87:522-531. doi:10.2527/jas.2008-1269

Peter, J. B., R. J. Barnard, V. R. Edgerton, C. A. Gillespie, and K. E. Stempel. 1972. Metabolic profiles of three fiber types of skeletal muscle in guinea pigs and rabbits. Biochemistry 11:2627-2633. doi:10.1021/bi00764a013

Rajas, F., A. Gautier-Stein, and G. Mithieux. 2019. Glucose-6 Phosphate, A Central Hub for Liver Carbohydrate Metabolism. Metabolites 9. doi:10.3390/metabo9120282

Reeves Pitts, M. A., H. R. Smith, E. C. Amerson, J. D. Starkey, C. W. Starkey, J. T. Sawyer, and T. D. Brandebourg. 2023. Feeding Ractopamine Improves the Growth Performance and Carcass Characteristics of the Lard-Type Mangalica Pig. Animals 13:3857.

Richter, E. A., and M. Hargreaves. 2013. Exercise, GLUT4, and skeletal muscle glucose uptake. Physiol Rev 93:993-1017. doi:10.1152/physrev.00038.2012

Riganti, C., E. Gazzano, M. Polimeni, E. Aldieri, and D. Ghigo. 2012. The pentose phosphate pathway: an antioxidant defense and a crossroad in tumor cell fate. Free Radic Biol Med 53:421-436. doi:10.1016/j.freeradbiomed.2012.05.006

Rimmer, L. A., E. R. Geisbrecht, M. D. Chao, T. G. O'Quinn, J. C. Woodworth, and M. D. Zumbaugh. 2024. Skeletal Muscle Metabolism Is Dynamic during Porcine Postnatal Growth. Metabolites 14:357.

Rolfs, Z., B. L. Frey, X. Shi, Y. Kawai, L. M. Smith, and N. V. Welham. 2021. An atlas of protein turnover rates in mouse tissues. Nat Commun 12:6778. doi:10.1038/s41467-021-26842-3

Sano, R., E. Tanaka, J. A. Korfage, G. E. Langenbach, N. Kawai, T. M. van Eijden, and K. Tanne. 2007. Heterogeneity of fiber characteristics in the rat masseter and digastric muscles. J Anat 211:464-470. doi:10.1111/j.1469-7580.2007.00783.x

Schiaffino, S., L. Gorza, S. Sartore, L. Saggin, S. Ausoni, M. Vianello, K. Gundersen, and T. Lomo. 1989. Three myosin heavy chain isoforms in type 2 skeletal muscle fibres. J Muscle Res Cell Motil 10:197-205. doi:10.1007/BF01739810

Schiaffino, S., and C. Reggiani. 2011. Fiber types in mammalian skeletal muscles. Physiol Rev 91:1447-1531. doi:10.1152/physrev.00031.2010

Soares, M. H., D. T. V. Junior, G. de Amorim Rodrigues, R. L. C. Junior, G. C. Rocha, B. M. Bohrer, M. Juarez, M. de Souza Duarte, and A. Saraiva. 2022. Effects of feeding ractopamine hydrochloride with or without supplemental betaine on live performance,

carcass and meat quality traits, and gene expression of finishing pigs. Meat Sci 191:108851. doi:10.1016/j.meatsci.2022.108851
Tokach, M. D., B. D. Goodband, and T. G. O'Quinn. 2016. Performance-enhancing technologies in swine production. Animal Frontiers 6:15-21. doi:10.2527/af.2016-0039
Valentino, T., V. C. Figueiredo, C. B. Mobley, J. J. McCarthy, and I. J. Vechetti, Jr. 2021. Evidence of myomiR regulation of the pentose phosphate pathway during mechanical load-induced hypertrophy. Physiol Rep 9:e15137. doi:10.14814/phy2.15137
Villee, C. A., V. K. White, and A. B. Hastings. 1952. Metabolism of C14 labeled glucose and pyruvate by rat diaphragm muscle in vitro. J Biol Chem 195:287-297.
Watkins, L. E., D. J. Jones, D. H. Mowrey, D. B. Anderson, and E. L. Veenhuizen. 1990. The effect of various levels of ractopamine hydrochloride on the performance and carcass characteristics of finishing swine. J Anim Sci 68:3588-3595. doi:10.2527/1990.68113588x
Yamasaki, M., K. Yamada, S. Furuya, J. Mitoma, Y. Hirabayashi, and M. Watanabe. 2001. 3-Phosphoglycerate dehydrogenase, a key enzyme for l-serine biosynthesis, is preferentially expressed in the radial glia/astrocyte lineage and olfactory ensheathing glia in the mouse brain. J Neurosci 21:7691-7704. doi:10.1523/JNEUROSCI.21-19-07691.2001
Zhang, L., Y. Zhou, W. Wu, L. Hou, H. Chen, B. Zuo, Y. Xiong, and J. Yang. 2017. Skeletal Muscle-Specific Overexpression of PGC-1alpha Induces Fiber-Type Conversion through Enhanced Mitochondrial Respiration and Fatty Acid Oxidation in Mice and Pigs. Int J Biol Sci 13:1152-1162. doi:10.7150/ijbs.20132

Chapter 2 - Beta-adrenergic agonists alter glucose and mitochondrial metabolite utilization independent of a fiber type shift

1. Introduction

The global population is projected to reach approximately 8.4 billion people by 2031 (Dohlman et al., 2022), increasing the number of people to feed but diminishing land and resources available for food production. This calls for the livestock industry to incorporate strategies that increase production efficiency without the need for more land and resources. Advancements in the industry, such as genetic selection, improved management, and nutritional changes have allowed for significant improvements in the past 3 decades. For example, carcass weight has increased 17% while feed consumption decreased by 4% (Tokach et al., 2016). Although these improvements are necessary for continued progress, innovative approaches are necessary to accommodate future demands with less resources. Understanding the biochemical pathways that skeletal muscle utilizes to metabolize nutrients in livestock species can aid in this effort to improve production efficiency.

Glycolysis and oxidative phosphorylation are the two main pathways through which skeletal muscle produces energy. Glycolysis produces a net of two ATP molecules, while oxidative phosphorylation can generate approximately 32 ATP molecules (Deshpande and Mohiuddin, 2024). However, carbon molecules are lost through certain reactions in the tricarboxylic acid (TCA) cycle. Alternatively, glycolysis preserves carbon molecules during ATP production, which can be recycled in the Cori cycle or to support for other anabolic processes. In fact, muscle of pigs classified with superior feed conversion ratios exhibit an upregulation of glycolytic enzymes and

suppression of oxidative enzymes compared to those from inferior feed conversion ratios (Fu et al., 2017). Therefore, livestock production performance is influenced by skeletal muscle metabolic characteristics.

Beta-adrenergic agonists (BAA) provide an ideal model to use the same genetics, nutrition, age, sex, and environmental conditions to initiate a metabolic shift. These pharmacological agents have been utilized to increase production efficiency in livestock animals since the 1990's. For example, ractopamine hydrochloride, a type of BAA, can increase average daily gain, feed efficiency, and loin eye area in finishing swine (Watkins et al., 1990; Carr et al., 2005; Panisson et al., 2020). Further, BAA feeding shifts muscle fiber type to a more glycolytic profile, which may contribute to BAA-mediated improvements in production efficiency (Depreux et al., 2002; Gunawan et al., 2007). Therefore, the objective of this study was to define the metabolic response of skeletal muscle to BAA feeding in finishing swine.

2. Materials and Methods

2.1 Animal Harvest and Sample Collection

The protocol used for this study was approved by the Kansas State Institutional Animal Care and Use Committee (protocol number 4485.52; approval date 07/28/2023). Pigs were housed at Kansas State University's Swine Unit. Twenty barrows (DNA 600 X 241; DNA Genetics, Columbus, NE, USA) were randomly selected for the trial. All pigs were fed a standard commercial diet containing 13% crude protein until the start of the trial. Five barrows were randomly placed into four pens for acclimation one week prior to the start of the study. Each pen was fitted with a single, dry self-feeder and nipple waterer. After the acclimation period, barrows were fed a standard corn-soybean meal commercial diet containing 16% crude protein with 0 g/ton (control) or 9 g/ton (BAA) ractopamine hydrochloride for 14 days. Individual backfat thickness

was measured using a Renco Lean-Meater Digital Backfat Indicator (Renco Corporation, Golden Valley, MN, USA) and body weights were recorded on d1 at the start of the trial, d8 (body weight only) and d14. After allotment of pigs to treatment groups, one pig died prior to the treatment feeding period and an additional pig died prior to the final data collection. This resulted in 8 control pigs (n=8) and 10 BAA pigs (n=10) being harvested over three days. Pigs from each group were transported to the Kansas State University Meat Lab and harvested on d14, d15, and d16. Samples from the *longissimus dorsi* (LD), *latissimus dorsi* (LAT), *semitendinosus* (ST), and *masseter* (MS) were collected within fifteen min of exsanguination. Portions of each muscle were snap frozen in liquid nitrogen, placed in cryomolds containing Tissue-Plus™ Optimal Cutting Temperature Compound (Fisher Scientific, Hampton, NH, USA) and frozen in isopentane cooled by liquid nitrogen for histology, or immediately processed for mitochondrial isolation. Snap frozen and histology samples were stored at –80 ˚C until further analysis.

2.2 Histochemistry

Muscle samples were cut twenty-five microns thick using a 550 HM micron (ThermoFisher Scientific, Waltham, MA, USA) and were placed on charged, saline-coated slides. The slides were placed in 3% hematoxylin (Fisher Scientific, Hampton, NH, USA) for 5 min then carefully rinsed with running deionized water for five min. Slides were then dipped once in 30% eosin (Fisher Scientific, Hampton, NH, USA) for 1 sec then rinsed with running deionized water for 2.5 min. Slides were then dipped in 50% and 70% ethanol for 10 sec each, then 95% and 100% for 30 sec each. Slides were then quickly dipped in zylene seven times, then dried with a kimwipe (Kimberly-Clark Professional Kimtech Science, Fisher Scientific, Hampton, NH, USA). The section was mounted with EprediaTM Shandon-Mount (Fisher Scientific, Hampton, NH, USA). Five images were taken of each slide with a 20x objective using a Nikon Eclipse Ti2 inverted microscope

(Nikon, Melville, NY, USA). Approximately 15 muscle fibers were measured per slide, which is an average of 75 measurements per muscle. Muscle fiber cross-sectional area was analyzed using Nikon-Elements software (Nikon, Melville, NY, USA). Values (μm^2) were averaged to obtain a single value for statistical analysis.

2.3 Mitochondrial Isolation

Mitochondria were isolated using the differential centrifugation method as described in Rimmer et al. (2024). Briefly, fresh muscle samples were collected and placed in ice-cold homogenization buffer (pH 7.4) containing 100 mM sucrose, 180 mM KCl, 50 mM Tris, 5 mM MgCl2, 10 mM EDTA, and 1 mM K-ATP at a 1.5:10 (wt/vol) ratio and then minced with scissors. Protease from *Bacillus licheniformis* (Cat #. 9014-01-1, Sigma Aldrich, St. Louis, MO, USA) was added to the tissue suspension at a final concentration of 0.4 mg/mL and homogenized using a Potter-Elvehjem tissue homogenizer system (Glas-Col, Terre Haute, IN, USA). Homogenates were diluted to 40 mL/g tissue with cold homogenization buffer and filtered through cheese cloth. The filtered homogenates were centrifuged at 2000 x *g* for 10 min at 4˚C, then supernatants were filtered through cheese cloth. Samples were centrifuged at 8000 x *g* for 10 min at 4˚C. The supernatant was removed, and the mitochondrial pellet was resuspended in a modified KHEB buffer (pH 7.2) containing 120 mM KCl, 0.2 mM KH2PO4, 1 mM HEPES, and 0.5 mM EGTA. Mitochondrial protein concentration was determined by Thermo Scientific™ Pierce™ BCA Protein Assay Kit (Pierce, Rockford, IL, USA) according to the manufacturer's instructions.

2.4 In Vitro [$^{13}C_3$]-Pyruvate Tracing in Isolated Mitochondria

Metabolite tracing was performed as described by Rimmer et al. (2024). Briefly, 3 mg of isolated mitochondria from section 2.3 were added to 1 mL of KHEB buffer containing 1 mM malic acid, 5 mM ADP, and 1 mM sodium pyruvate-$^{13}C_3$ (Sigma Aldrich, St. Louis, MO, USA).

Tracing control reactions were incubated with 1 mM sodium pyruvate. Samples were incubated at 37˚C on a rocker at 40 rpm for 45 min. Samples were mixed with 2 M perchloric acid, incubated on ice for 15 min, and centrifuged at 12,000× *g* at 4˚C for 5 min. The supernatant was transferred to new tubes, neutralized with 3 M KOH, and stored at −80˚C until further analysis.

2.5 Mass Spectrometry of Metabolites

Samples and TCA intermediate standards were prepared for gas chromatography-mass spectrometry (GC-MS) using the deproteinization and derivatization method described in Rimmer et al. (2024) and Matarneh et al. (2021). Briefly, 5 M of hydroxylamine hydrochloride was added to samples followed by 4 M KOH and then sonicated at 65˚C for 60 min. Samples were acidified with 6 N HCl, saturated with NaCl, and the organic phase of the sample was separated by ethyl acetate after centrifugation. The organic supernatant was extracted and evaporated to dryness under a continuous stream of N_2 at 40 ˚C. Equal parts N-tert-butyldimethylsilyl-N-methyltrifluoroacetamide (MTBSTFA) and ethyl acetate were added to the dried sample and incubated at 65 ˚C for 1 hr to form tertiary-butyldimethylsilyl (tBDMS) derivatives. Samples were separated using gas chromatography (Agilent 6890N; Agilent, Santa Clara, CA, USA) on a J&W HP-5 ms GC Column (HP-5MS, 30 m, 0.25 mm, 0.25 μm film; Agilent Technologies), as previously described in Rimmer et al. (2024) and El-Kadi et al. (2009). Intermediate ions were evaluated based on their mass-to-charge ratio (*m/z*) using the single ion monitoring method with a mass spectrophotometer (Agilent 5973N; Agilent, Santa Clara, CA, USA). The ions monitored included the following: pyruvate (274.10); succinate (289.10); fumarate (287.10); malate (419.20); oxaloacetate (432.10); α-ketoglutarate (446.20); and citrate (591.40). The mole percent excess (MPE) was determined through the peak area and was calculated as (M + i/M + 0) × 100, where M + i was defined as the isotopic enrichment of a molecule.

2.6 Western Blotting

Muscle samples were powdered in liquid nitrogen. IntactProtein™ lysis buffer (GenuIN Biotech, Blacksburg, VA, USA) was added to 100 mg powdered sample and homogenized according to manufacturer's instructions. Samples were incubated on ice for 15 min and then centrifuged at 13,000 g at 4°C for 10 min. The supernatant was extracted and heated at 95°C for 5 min. Protein concentration was measured using a BCA Protein Assay Kit. Samples were diluted to a final concentration of 3 mg/mL using IntactProtein™ lysis buffer and 2x Laemmli Sample Buffer containing SDS, glycerol, bromophenol blue, tris-hydrochloride (pH 6.8), protease inhibitor mini tablets (Cat# PIA32955, Fisher Scientific, Hampton, NH, USA), and β-mercaptoethanol. Samples prepared for myosin heavy chain detection were prepared with 2M DTT instead of β-mercaptoethanol. Equal amounts of protein were separated using SDS-PAGE, transferred to PVDF or nitrocellulose membranes, and blocked at RT using OneBlock™ Western-CL or -FL blocking buffer, respectively (Prometheus Protein Biology Products, Genesee Scientific, San Diego, CA, USA). Membranes were incubated overnight at 4°C with their corresponding primary antibody. The following day, membranes were incubated with the appropriate secondary antibody for 1 hr. The following proteins were detected using the conditions as follows (primary antibody, primary antibody concentration, blocking time, secondary antibody, secondary antibody concentration, and imaging methodology): pyruvate carboxylase [anti-pyruvate carboxylase (Cat# NBP1-49536, Novus Biologicals, Centennial, CO, USA), 1:1,000, 2 hr, Goat anti-Rabbit IgG (H+L) Secondary Antibody, HRP, Invitrogen™ (Cat# 31460, Fisher Scientific, Hampton, NH, USA), 1:8,000, chemiluminescence]; succinate dehydrogenase [anti-SDHα (Cat# NBP2-93922, Novus Biologicals, Centennial, CO, USA), 1:1,000, 30 min, Goat anti-Rabbit IgG (H+L) Highly Cross-Adsorbed Secondary Antibody, Alexa Fluor™ Plus 555,

Invitrogen™ (Cat# A32732, Fisher Scientific, Hampton, NH, USA), 1:8,000, fluorescence]; lactate dehydrogenase [anti-LDHα (Cat # NBP2-19320, Novus Biologicals, Centennial, CO, USA), 1:1,000, 30 min, Goat anti-Rabbit IgG (H+L) Highly Cross-Adsorbed Secondary Antibody, Alexa Fluor™ Plus 555, Invitrogen™ (Cat# A32732, Fisher Scientific, Hampton, NH, USA), 1:8,000, fluorescence]; SC71 [MyHC Type IIa, IgG1 (DSHB, Iowa City, IA, USA), 0.5 μg/mL, 1 hr, Goat anti-Mouse IgG (H+L) Cross-Adsorbed Secondary Antibody, Alexa Fluor™ 555, Invitrogen™ (Cat# A21422, Fisher Scientific, Hampton, NH, USA), 1:10,000, fluorescence]; 10F5 [MyHC Type IIb, IgM (DSHB, Iowa City, IA, USA), 0.5 μg/mL, 1 hr, Goat anti-Mouse IgM (Heavy chain) Secondary Antibody, Alexa Fluor™ 647, Invitrogen™ (Cat# A21238, Fisher Scientific, Hampton, NH, USA), 1:10,000, fluorescence]; BAF8 + 6H1 cocktail [MyHC Type I, IgG2b + MyHC Type IIx, IgM (DSHB, Iowa City, IA, USA), 0.5 μg/mL, 1 hr, Goat anti-Mouse IgG2b Cross-Adsorbed Secondary Antibody, Alexa Fluor™ 488, Invitrogen™ (Cat# A21141, Fisher Scientific, Hampton, NH, USA) + Goat anti-Mouse IgM (Heavy chain) Secondary Antibody, Alexa Fluor™ 647, Invitrogen™ (Cat# A21238, Fisher Scientific, Hampton, NH, USA), 1:10,000, fluorescence]. Prior to chemiluminescent imaging, Prosignal Pico ECL reagent (Prometheus Protein Biology, Genesee Scientific, San Diego, CA, USA) was added to the membranes for 45 s and then removed for imaging using the IBright Imaging System (ThermoFisher Scientific, Waltham, MA, USA). Invitrogen™ No-StainTM Protein labeling reagent (ThermoFisher Scientific, Walham, MA, USA) was used to measure total protein abundance according to the manufacturer's instructions. Images were analyzed using Thermo Fisher iBright Analysis Software and normalized to the total protein abundance.

2.7 Phosphofructokinase Activity

Samples were prepared by adding 100 mM K_2HPO_4, pH 7.4, to 20 mg powdered muscle. Samples were then homogenized, placed in an ice bath for 15 min, and centrifuged at 13,000 g for 10 min at 4˚C. The supernatant was transferred to a new tube, and each sample received buffer containing 120 mM MES, 3.2 mM $MgSO_4 \cdot 7H_2O$, 2 mM K-ATP, 1 mM NADH, and 3 mM fructose-6-phosphate (Cat# F3627, Sigma Aldrich, St. Louis, MO, USA). An enzyme solution containing 1.2 U glycerol-3-phosphate dehydrogenase (Cat# 10127752001, Sigma Aldrich, St. Louis, MO, USA), 0.12 U triosephosphate isomerase (Cat# T2391, Sigma Aldrich, St. Louis, MO, USA), and 1 U aldolase (Cat# A2714**,** Sigma Aldrich, St. Louis, MO, USA) was added to each sample containing buffer. Samples were then plated in triplicate on a 96-well plate. The absorbance (OD) was measured at 339 nm every minute for 11 min. Slopes of each reaction were obtained when R-squared (RSQ) values were greater than 0.99.

2.8 Lactate and Glucose Concentration

Muscle samples were powdered in liquid nitrogen, and 100 mg frozen muscle was homogenized in 0.5 M perchloric acid. Following a 15 min incubation on ice and centrifugation at 13,000 g for 10 min at 4˚C, 200 µL of 2M KOH was added to the homogenate. Glucose and lactate concentration was measured based on the methods described in Hammelman et al. (2003) with some modifications. To measure glucose, samples were diluted 1:2 in a buffer containing 62.5 mM triethanolamine, 25 mM EDTA, 35 mM $MgCl_2$ and 1.3 mM NADP in a glass tube. Samples were plated in triplicate in a 96-well plate and absorbance (OD_1) was measured at 340 nm. Each tube received 1.9 U glucose-6-phosphate dehydrogenase (Cat# 10165875001, Sigma Aldrich, St. Louis, MO, USA), incubated at RT for 20 min, and plated in triplicate on a 96-well plate to measure absorbance (OD_2). After the addition of 0.95 U hexokinase (Cat#: 11426362001, Sigma Aldrich,

St. Louis, MO, USA) and 11 mg/mL Na-ATP to each tube, samples were incubated for 20 min at RT and plated in triplicate in a 96-well plate to measure absorbance (OD_3). Glucose-6-phosphate was determined by $OD_2 - OD_1$ calculated using a standard curve. Glucose was determined by $OD_3 - OD_1$ and calculated using a standard curve. To measure lactate, samples were diluted 1:4 in a buffer containing 0.125 M HCl, 473 mM glycine, 2.92 mM β-Nicotinamide adenine dinucleotide sodium salt, and 2.73% hydrazine in a glass tube. Samples were plated in triplicate in a 96-well plate and absorbance (OD_1) was measured at 340 nm. Each tube received 1.75 U lactate dehydrogenase (Cat# L2625, Sigma Aldrich, St. Louis, MO, USA), incubated at RT for 90 min, and was plated in triplicate on a 96-well plate to measure absorbance (OD_2). Lactate was determined by $OD_2 - OD_1$ and calculated using a standard curve.

2.9 Statistics Section

The data were analyzed as a split plot design with treatment as the whole plot factor and muscle as the sub plot factor. Data were considered significant when $p \leq 0.05$ and the means were separated by pairwise comparisons. Main effect means (muscle or treatment) are reported when the interaction was not significant (muscle × treatment). Data are presented as the least squares means +/− standard error. All data were analyzed using R (version 4.2.1, Indianapolis, IN, USA). Western blot data were log transformed to normalize the residuals. Data are presented as the back-transformed values.

3. Results

At the end of finishing, barrows were either fed a commercial diet with 16% crude protein containing 0 g/ton (control) or 9 g/ton ractopamine hydrochloride (BAA) for 2 wks to evaluate the BAA-mediated metabolic response in skeletal muscle. Individual body weights were measured at the start of BAA feeding (d0), d8, and d14. Backfat thickness was determined using an ultrasound

on d0 and d14. Pigs were harvested over three days for carcass measurements and sample collection. Four muscles with inherently different metabolic profiles were collected for analysis, including the LD (glycolytic muscle), LAT (mixed muscle), red portion of the ST (mixed muscle), and MS (oxidative muscle).

3.1 Live Animal and Carcass Data

Body weight and backfat depth were measured during BAA feeding to evaluate the phenotypic response to ractopamine hydrochloride. There was no difference between control and BAA pigs at all timepoints evaluated throughout feeding (Table 1). Carcass data were collected after harvest. There were no differences in hot carcass weight (Figure 2.1A), dressing percentage (Figure 2.1B), backfat thickness (Figure 2.1C), or loin eye area (Figure 2.1D).

	Day		
Measurement	1	8	14
BW, Control (lbs)	287.72 ± 3.17	289.44 ± 3.17	312.17 ± 3.17
BW, BAA (lbs)	278.25 ± 3.17	285.08 ± 3.17	304.54 ± 3.17
BF, Control (mm)	11.2 ± 0.422	N/A	12.2 ± 0.422
BF, BAA (mm)	12.9 ± 0.422	N/A	13.8 ± 0.422

Table 1. Body weight and backfat measurements during BAA feeding. Live weight of each group on d1, d8, and d14 and backfat (BF) depth of each group on d1 and d14. Skin thickness is included in BF measurement. There were no differences between treatment groups within each timepoint. Data are shown as means ± SE. Ten BAA barrows (n = 10) and eight control barrows (n = 8) per group.

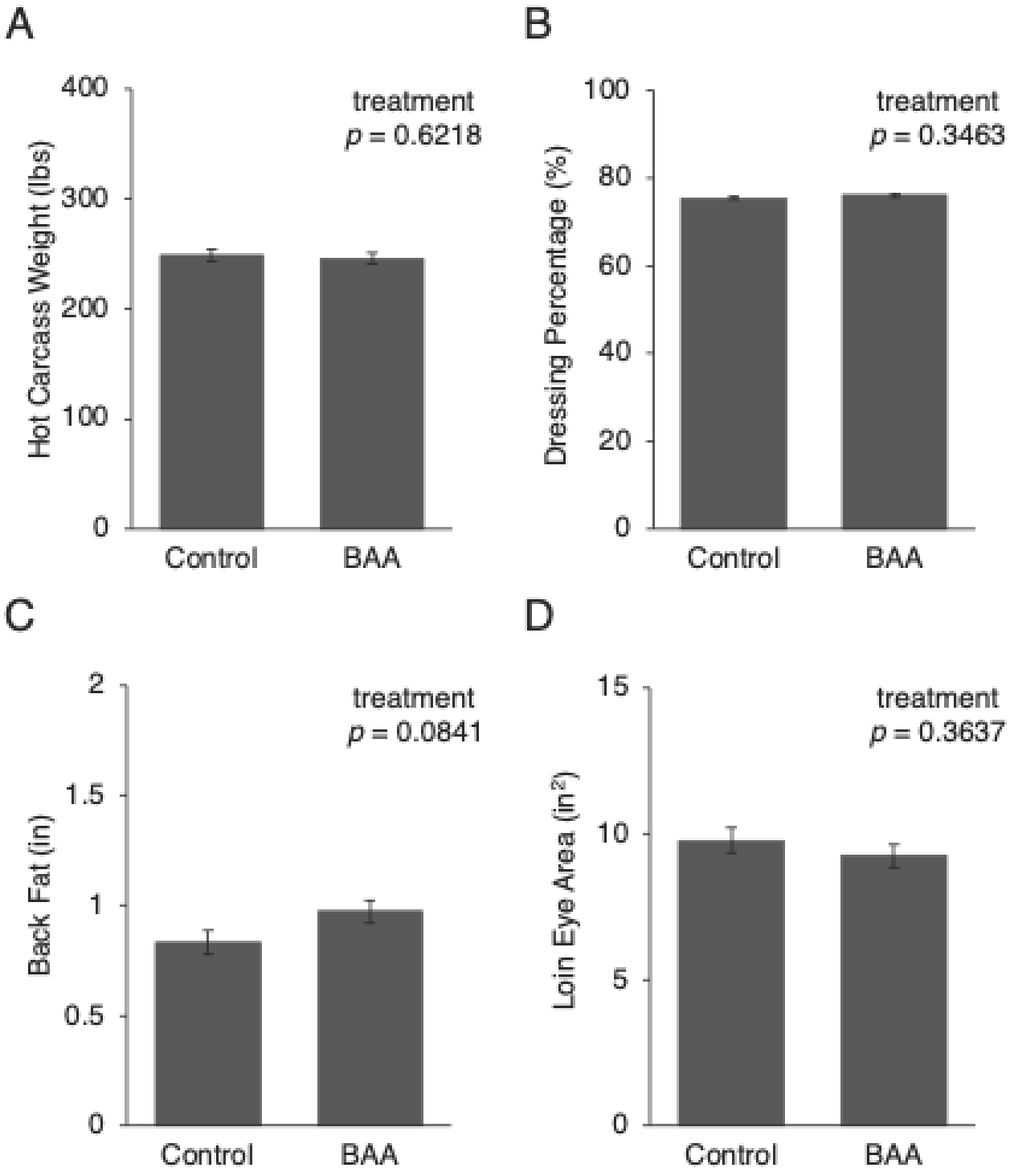

Figure 2.1. Evaluation of carcasses from control and BAA pigs. (A) Hot carcass weight, (B) dressing percentage (hot carcass weight ÷ live weight × 100), (C) backfat thickness, and (D) loin eye area of carcasses from each treatment. Data are shown as means ± SE. Ten BAA barrows (n = 10) and eight control barrows (n = 8) per group.

3.2 Muscle Cross-Sectional Area

Muscle cross-sectional area (CSA) was measured to determine if BAA feeding stimulated muscle hypertrophy. All muscles evaluated differed in CSA with ST > LD > LAT > MS (Figure 2.2A; $p < 0.05$). However, there were no treatment differences in CSA (Figure 2.2B).

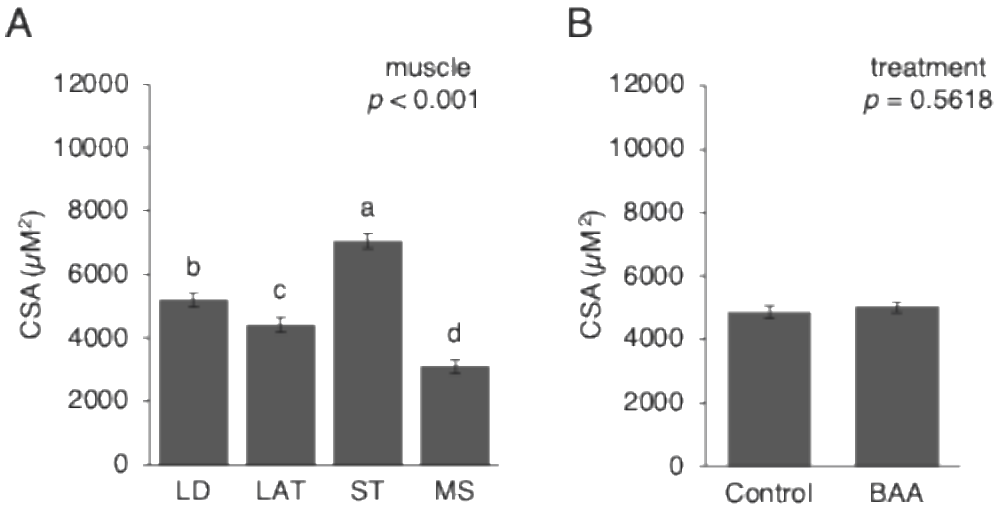

Figure 2.2. Assessment of muscle fiber size. **(A-B)** Muscle cross-section area (CSA) of **(A)** LD, LAT, ST, and MS muscles, and **(B)** from different treatment groups. Data are shown as means ± SE. Ten BAA barrows (n = 10) and eight control barrows (n = 8) per group. Means lacking a common letter (a, b, c, d) differ ($p < 0.05$).

3.3 Myosin Heavy Chain Isoforms

To classify muscles evaluated and determine if BAA supplementation induced a fiber type shift, protein abundance of myosin heavy chain (MyHC) isoforms were assessed. Fiber types I, IIa, IIx, and IIb correspond to expression of MyHC isoforms I, IIa, IIx, and Ib, respectively (Pette and Staron, 2000). Protein abundance of MyHC I was highest in the MS, intermediate in the LAT, and lowest in the ST and LD (Figure 2.3A; $p < 0.05$). The MS had the highest protein abundance of MyHC IIa compared to other muscles (Figure 2.3D; $p < 0.05$), while MyHC IIx was lowest in the MS compared to other muscles (Figure 2.3G, $p < 0.05$). Protein abundance of MyHC IIb was lowest in the MS, intermediate in the LD and LAT, and highest in the ST (Figure 2.3J; $p < 0.05$). However, there were no treatment differences in MyHC protein abundance (Figure 2.3B, E, H, K).

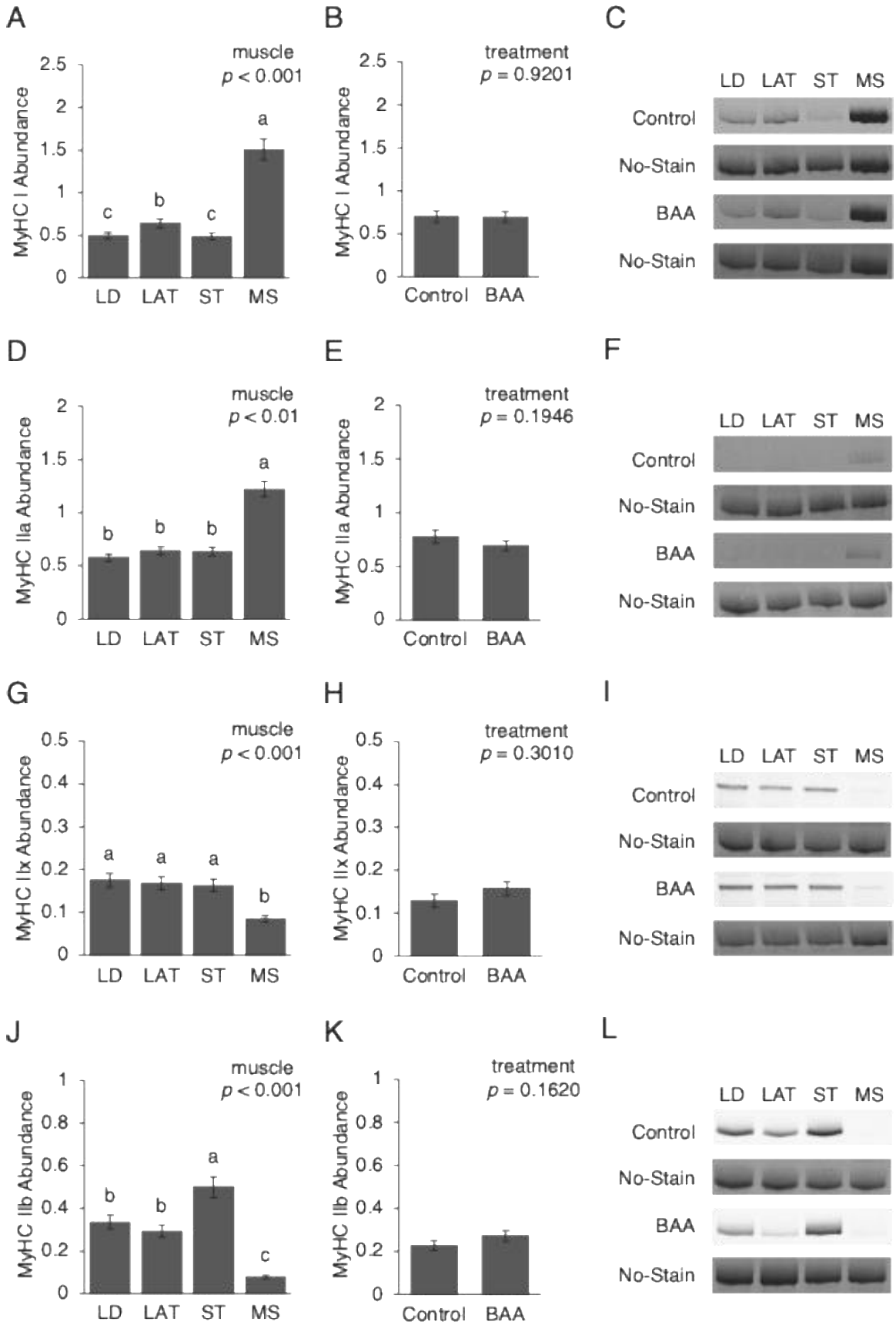
A
muscle
p < 0.001
MyHC I Abundance
2.5
2
1.5
1
0.5
0
c
b
c
a
LD LAT ST MS
B
treatment
p = 0.9201
MyHC I Abundance
Control BAA
C
LD LAT ST MS
Control
No-Stain
BAA
No-Stain
D
muscle
p < 0.01
MyHC IIa Abundance
b
b
b
a
E
treatment
p = 0.1946
MyHC IIa Abundance
F
G
muscle
p < 0.001
MyHC IIx Abundance
0.5
0.4
0.3
0.2
0.1
a
a
a
b
H
treatment
p = 0.3010
MyHC IIx Abundance
I
J
muscle
p < 0.001
MyHC IIb Abundance
1
0.8
0.6
0.4
0.2
b
b
a
c
K
treatment
p = 0.1620
MyHC IIb Abundance
L

Figure 2.3. Relative abundance of myosin heavy chain isoforms. **(A-B)** Relative abundance of MyHC I in each **(A)** muscle and **(B)** treatment group. **(C)** Representative images of Western blots quantified in **(A-B)**. **(D-E)** Relative abundance of MyHC IIa in each **(D)** muscle and **(E)** treatment group. **(F)** Representative images of Western blots quantified in **(D-E)**. **(G-H)** Relative abundance of MyHC IIx in each **(G)** muscle and **(H)** treatment group. **(I)** Representative images of Western blots quantified in **(G-H)**. **(J-K)** Relative abundance of MyHC IIb in each **(J)** muscle and **(K)** treatment group. **(L)** Representative images of Western blots quantified in **(J-K)**. Data are shown as means ± SE. Ten BAA barrows (n = 10) and eight control barrows (n = 8) per group. Means lacking a common letter (a, b, c) differ ($p < 0.05$).

3.4 Glycolytic Metabolites and Enzymes

In addition to characterizing the metabolic profile of muscles through abundance of MyHC isoforms, glycolytic intermediates and enzymes were measured to evaluate changes in glycolysis that may occur without altering MyHC isoforms present. For example, glucose is phosphorylated to produce glucose-6-phosphate (G6P) after entering the cell to facilitate additional glucose uptake. A subsequent regulatory step of glycolysis is catalyzed by phosphofructokinase (PFK) to produce fructose 1,6-bisphosphate and an increase in its activity is indicative of increased glycolytic flux. Further, lactate dehydrogenase (LDHα) is upregulated and supports the conversion of pyruvate to lactate, a process upregulated in glycolytic muscles (Peter et al., 1972). Lactate can then be used in the Cori cycle where it is shuttled to the liver and converted to glucose via gluconeogenesis. Similarly, lactate concentration corresponds to glycolytic capacity and utilization of the Cori cycle. Therefore, concentrations of glucose, G6P, and lactate were measured as well as PFK activity and LDHα abundance to evaluate altered glycolytic capacity.

Activity of PFK was the highest in the ST, intermediate in the LD and LAT, and lowest in the MS (Figure 2.4A; $p < 0.05$). There were no differences in PFK activity between treatment groups (Figure 2.4B). Further, abundance of LDHα was highest in the ST, intermediate in the LD and LAT, and lowest in the MS (Figure 2.4C; $p < 0.05$). However, there were no differences in LDHα between treatment groups (Figure 2.4D). Glucose concentration was higher in LD and LAT

and lowest in the ST and MS (Figure 2.4F; $p < 0.05$). Muscles of control pigs had exhibited an increase in glucose concentration compared to muscles of BAA pigs (Figure 2.4G; $p < 0.05$). In addition, G6P levels were highest in the LD, intermediate in the LAT, and lowest in the ST and MS (Figure 2.4H; $p < 0.05$). Muscles of control pigs had higher amounts of G6P compared to BAA pigs (Figure 2.4I, $p < 0.05$). Although lactate concentration was highest in the LAT followed by LD, ST, and MS muscles (Figure 2.4J; $p < 0.05$), there were no differences between treatment groups (Figure 2.4K). These data suggest glycolytic metabolite utilization is altered in muscles of BAA pigs while activity and abundance of commonly evaluated glycolytic enzymes remain unchanged.

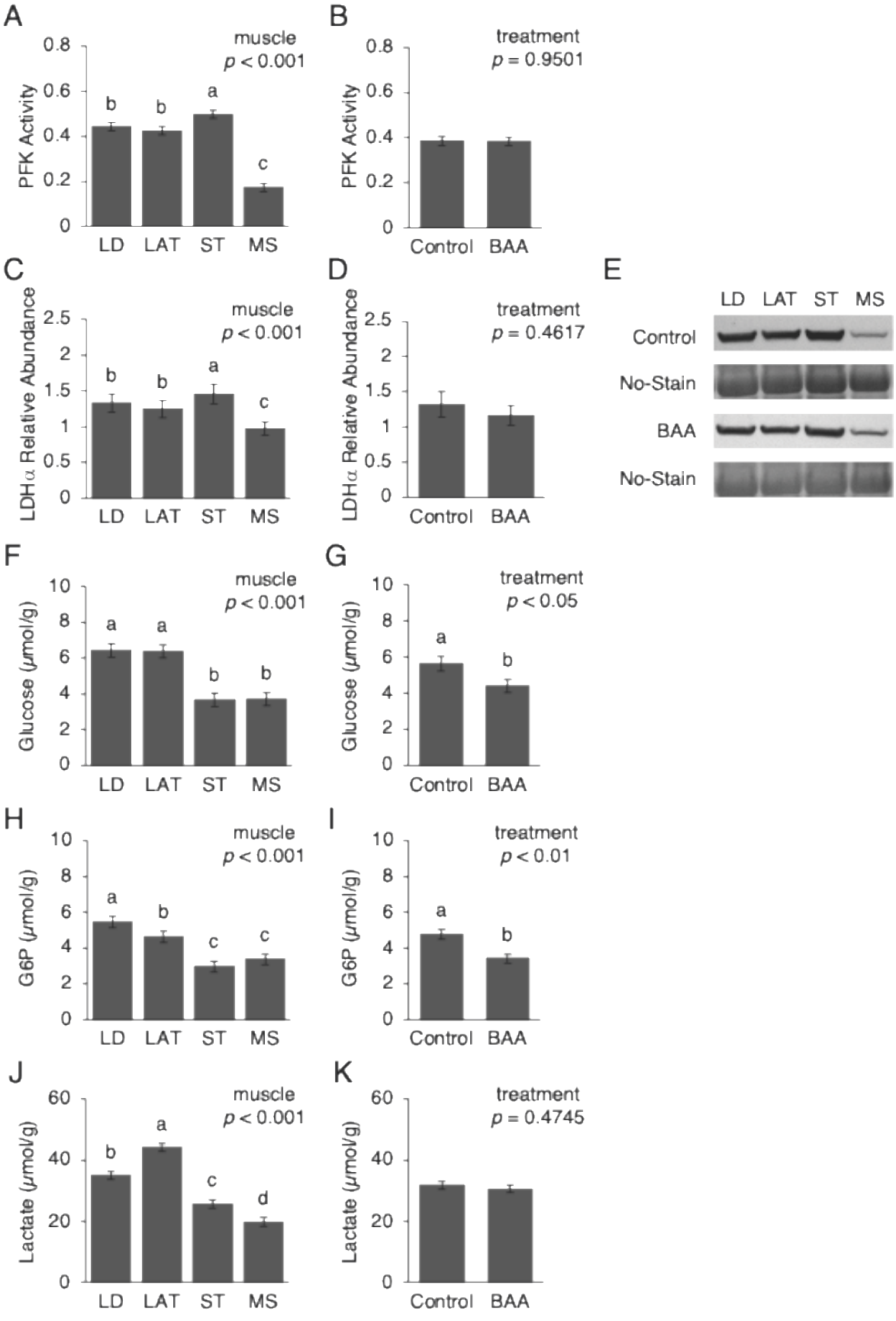
A
muscle
p < 0.001
PFK Activity
0.8
0.6
0.4
0.2
0
b
b
a
c
LD LAT ST MS
B
treatment
p = 0.9501
PFK Activity
0.8
0.6
0.4
0.2
0
Control BAA
C
muscle
p < 0.001
LDHα Relative Abundance
2.5
2
1.5
1
0.5
0
b
b
a
c
LD LAT ST MS
D
treatment
p = 0.4617
LDHα Relative Abundance
2.5
2
1.5
1
0.5
0
Control BAA
E
LD LAT ST MS
Control
No-Stain
BAA
No-Stain
F
muscle
p < 0.001
Glucose (μmol/g)
10
8
6
4
2
0
a
a
b
b
LD LAT ST MS
G
treatment
p < 0.05
Glucose (μmol/g)
10
8
6
4
2
0
a
b
Control BAA
H
muscle
p < 0.001
G6P (μmol/g)
10
8
6
4
2
0
a
b
c
c
LD LAT ST MS
I
treatment
p < 0.01
G6P (μmol/g)
10
8
6
4
2
0
a
b
Control BAA
J
muscle
p < 0.001
Lactate (μmol/g)
60
40
20
0
b
a
c
d
LD LAT ST MS
K
treatment
p = 0.4745
Lactate (μmol/g)
60
40
20
0
Control BAA

Figure 2.4. Enzymes and metabolites indicative of glycolytic metabolism. **(A-B)** Relative abundance of lactate dehydrogenase α (LDHα) in each **(A)** muscle and **(B)** treatment group. **(C)** Representative images of Western blots quantified in **(A-B)**. **(D-E)** Concentration of lactate in each **(D)** muscle and **(E)** treatment group. **(F-G)** Activity of phosphofructokinase (PFK) in each **(F)** muscle and **(G)** treatment group. **(H-I)** Concentration of glucose 6-phosphate (G6P) in each **(H)** muscle and **(I)** treatment group. **(J-K)** Concentration of glucose in each **(J)** muscle and **(K)** treatment group. Data are shown as means ± SE. Ten BAA barrows (n = 10) and eight control barrows (n = 8) per group. Means lacking a common letter (a, b, c, d) differ ($p < 0.05$).

3.5 Oxidative Enzymes

Enzymes involved in the TCA cycle were also evaluated to assess changes in oxidative metabolism in BAA muscle. After glucose is converted to pyruvate in glycolysis, pyruvate can enter the TCA cycle through the pyruvate dehydrogenase complex (PDH) or pyruvate carboxylase (PC). While PDH catalyzes the conversion of pyruvate to acetyl-CoA, NADH, and CO_2, PC can produce oxaloacetate using pyruvate, ATP, and a bicarbonate molecule. While mechanisms that drive pyruvate entry route are still being investigated, this may be an adaptive mechanism to conserve carbon backbones for anabolic processes. Further, succinate is converted to fumarate by succinate dehydrogenase-α (SDHα) and its abundance is associated with an increase in oxidative capacity (Essen et al., 1975).

Abundance of SDHα was highest in the MS, intermediate in the LAT and ST, and lowest in the LD (Figure 2.5A; $p < 0.05$). There was no difference in treatment. The abundance of PC was highest in the LAT, intermediate in the ST and MS, and lowest in the LD (Figure 2.5D; $p < 0.05$). The abundance of PC was higher in the control group than the treatment group (Figure 2.5E; $p < 0.05$).

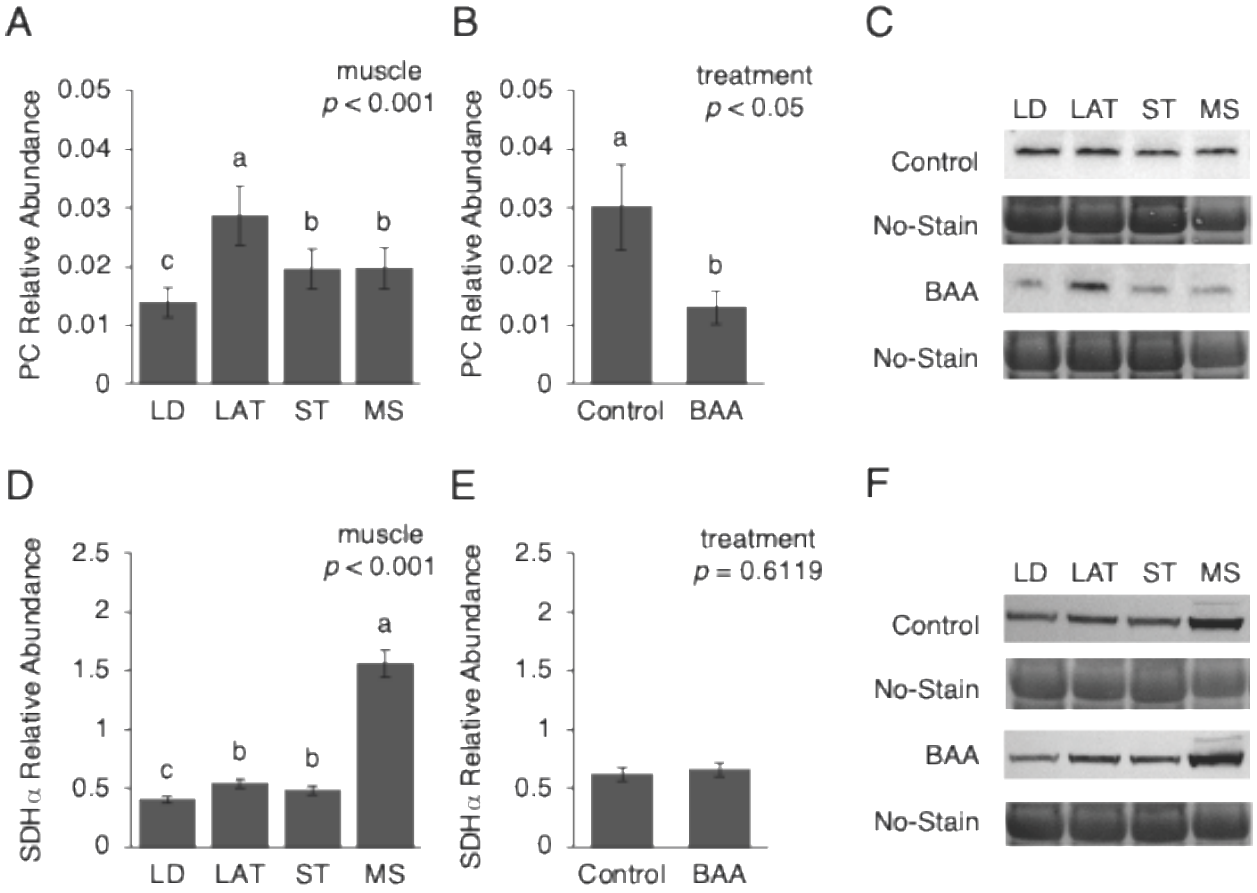

Figure 2.5. Enzymes indicative of oxidative metabolism. **(A-B)** Relative abundance of succinate dehydrogenase-α (SDHα) in each **(A)** muscle and **(B)** treatment group. **(C)** Representation of Western blots quantified in **(A-B)**. **(D-E)** Relative abundance of pyruvate carboxylase (PC) in each **(D)** muscle and **(E)** treatment group. **(F)** Representative images of Western blots quantified in **(D-E)**. Data are shown as means ± SE. Ten BAA barrows (n = 10) and eight control barrows (n = 8) per group. Means lacking a common letter (a, b, c) differ ($p < 0.05$).

3.6 Mitochondrial metabolite utilization

Under the conditions of BAA supplementation herein, minimal changes in protein abundance were observed. However, utilization of glucose is altered in muscle of BAA pigs. Therefore, an *in vitro* metabolite tracing approach in isolated mitochondria was implemented to determine if pyruvate utilization is altered in muscle of BAA pigs. Isolated mitochondria from control and BAA muscles were incubated with [$^{13}C_3$]-pyruvate and unlabeled malate, and enrichment of isotopomers was determined using gas chromatography-mass spectrometry. Values

represent M + i, where i denotes the number of ^{13}C contained in the intermediate. It is important to note this approach depicts the number of ^{13}C in each TCA cycle intermediate rather than total amount of each intermediate. For example, M + 2 indicates two ^{13}C are present in the intermediate. Labeling patterns of isotopomers can be traced through the TCA cycle and theoretical representations of ^{13}C are depicted in Figure 2.6.

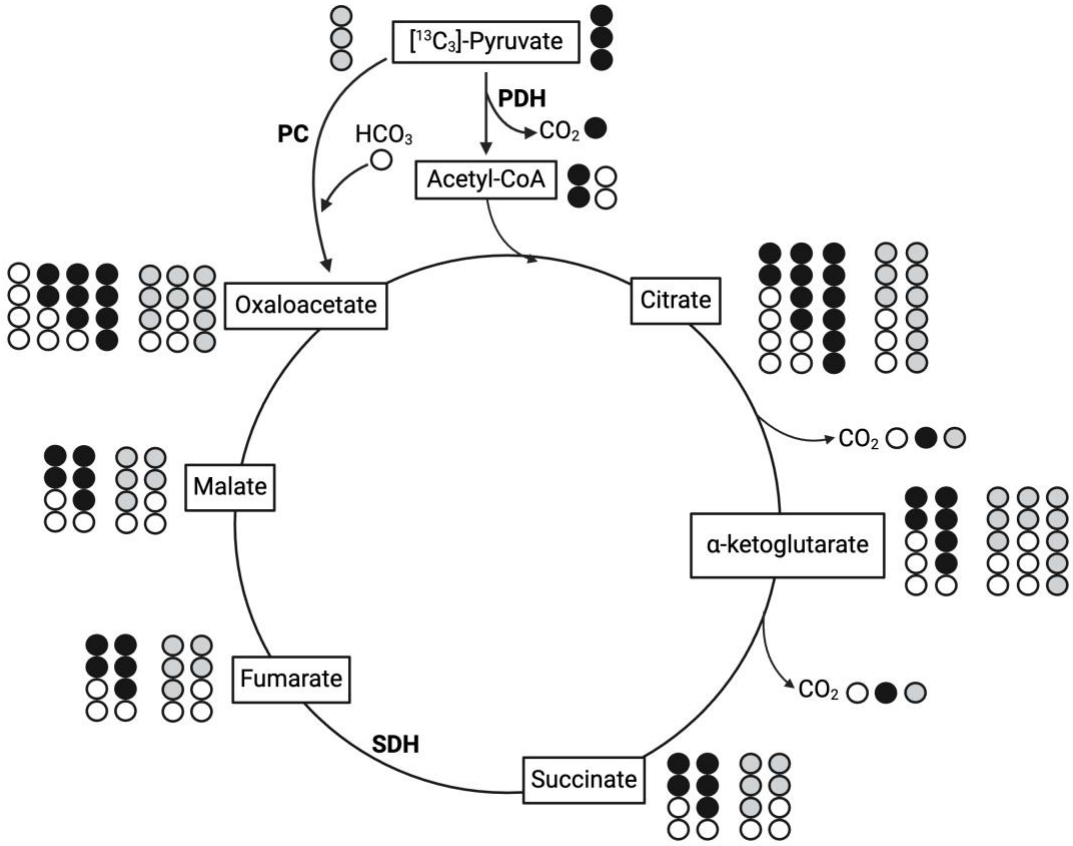

Figure 2.6. Schematic depicting theoretical enrichment patterns of TCA cycle intermediates derived from [$^{13}C_3$]-pyruvate. Black circles represent ^{13}C that enter the TCA cycle via PDH. Grey circles represent ^{13}C that enter the TCA cycle through PC. White circles represent unlabeled carbons (^{12}C).

Oxaloacetate (OAA) M + 2 increased in BAA LAT mitochondria compared to BAA MS mitochondria, but there were no differences in OAA M + 2 in LAT and MS mitochondria of control pigs (Figure 2.7A*; p* < 0.05). Further, OAA M + 3 and M + 4 increased in LAT compared to MS

regardless of treatment (Figure 2.7B-C; $p < 0.05$). Citrate M + 2, M + 3, and M + 4 (Figure 2.8A-C; $p < 0.05$) as well as α-ketoglutarate M + 4 and M + 5 (Figure 2.9F-G; $p < 0.05$) increased in control LAT mitochondria compared to all other mitochondria. Citrate M + 6 (Figure 2.8D; $p < 0.05$) as well as α-ketoglutarate M + 2 and M + 3 (Figure 2.9D-E; $p < 0.05$) increased in control mitochondria regardless of treatment. Although citrate M + 6 did not differ between muscles, alpha-ketoglutarate M + 2 and M + 3 was increased in LAT mitochondria compared to LD and MS mitochondria regardless of treatment (Figure 2.9A-C; $p < 0.05$). These data suggest BAA mitochondria exhibit altered utilizing of pyruvate, the glycolytic end product, compared to control mitochondria. Further, LAT mitochondria may respond differently than mitochondria from other muscles evaluated.

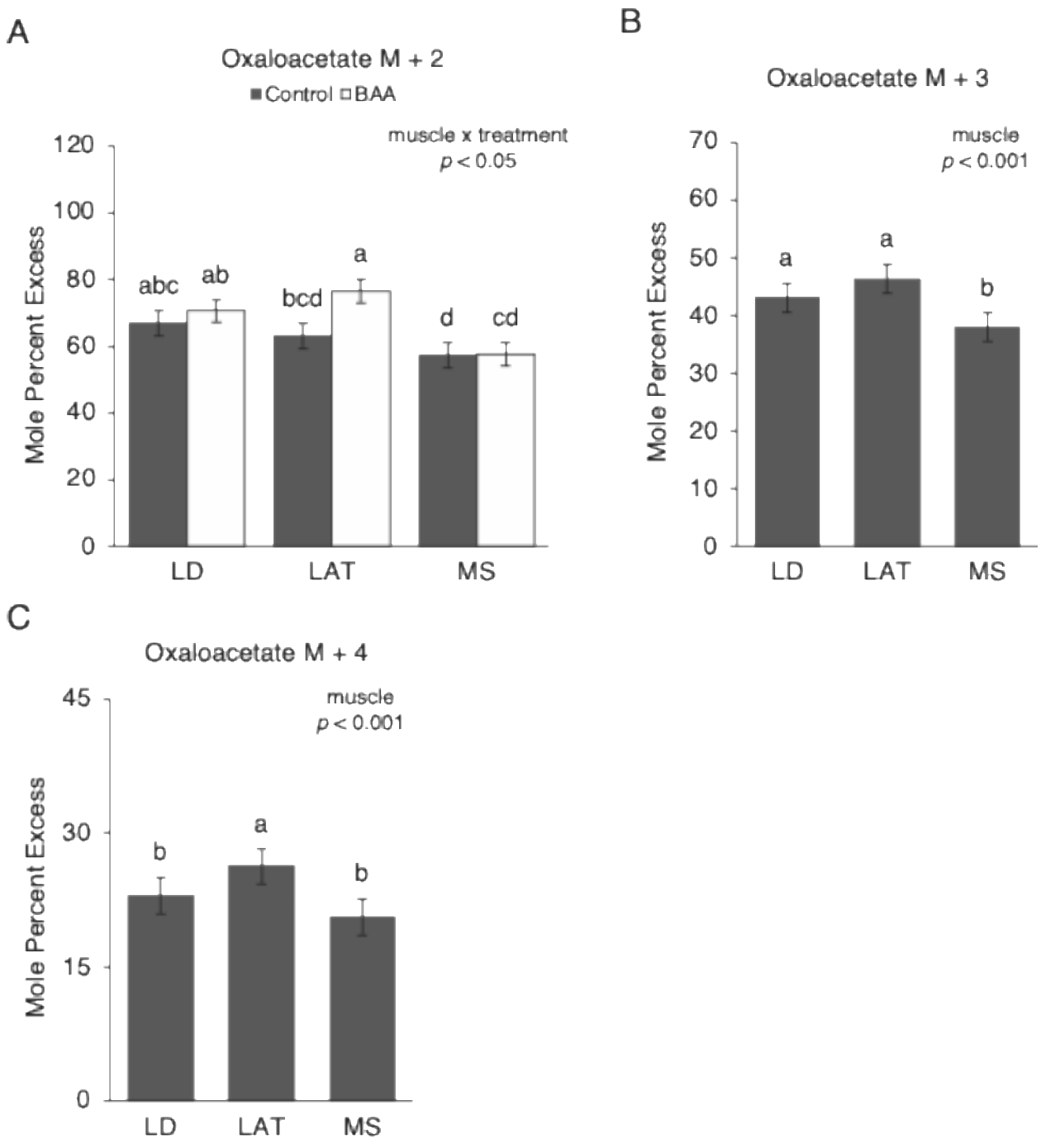

Figure 2.7. Enrichments of oxaloacetate from [$^{13}C_3$]-pyruvate in isolated mitochondria. Enrichments of oxaloacetate from [$^{13}C_3$]-pyruvate in isolated mitochondria. Enrichment of (**A**) M + 2, (**B**) M + 3, and (**C**) M + 4 oxaloacetate in LD, LAT and MS mitochondria isolated from control and BAA pigs. Data are shown as means ± SE. Ten BAA barrows (n = 10) and eight control barrows (n = 8) per group. Means lacking a common letter (a, b, c, d) differ ($p < 0.05$).

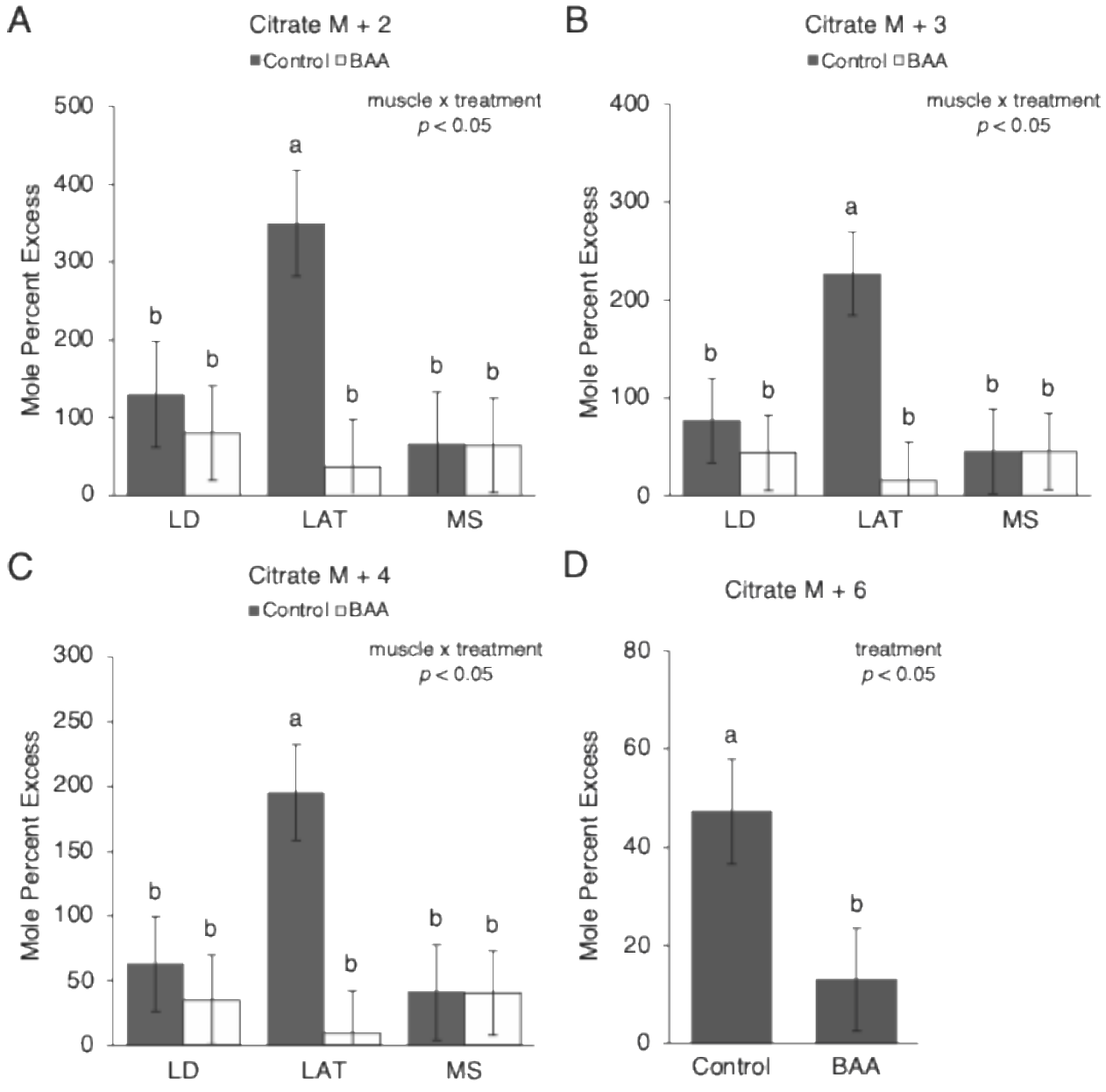

Figure 2.8. Enrichments of citrate from [$^{13}C_3$]-pyruvate in isolated mitochondria. Enrichment of **(A)** M + 2, **(B)** M + 3, **(C)** M + 4, and **(D)** M + 6 citrate in LD, LAT and MS mitochondria isolated from control and BAA pigs. Data are shown as means ± SE. Ten BAA barrows (n = 10) and eight control barrows (n = 8) per group. Means lacking a common letter (a, b) differ ($p < 0.05$).

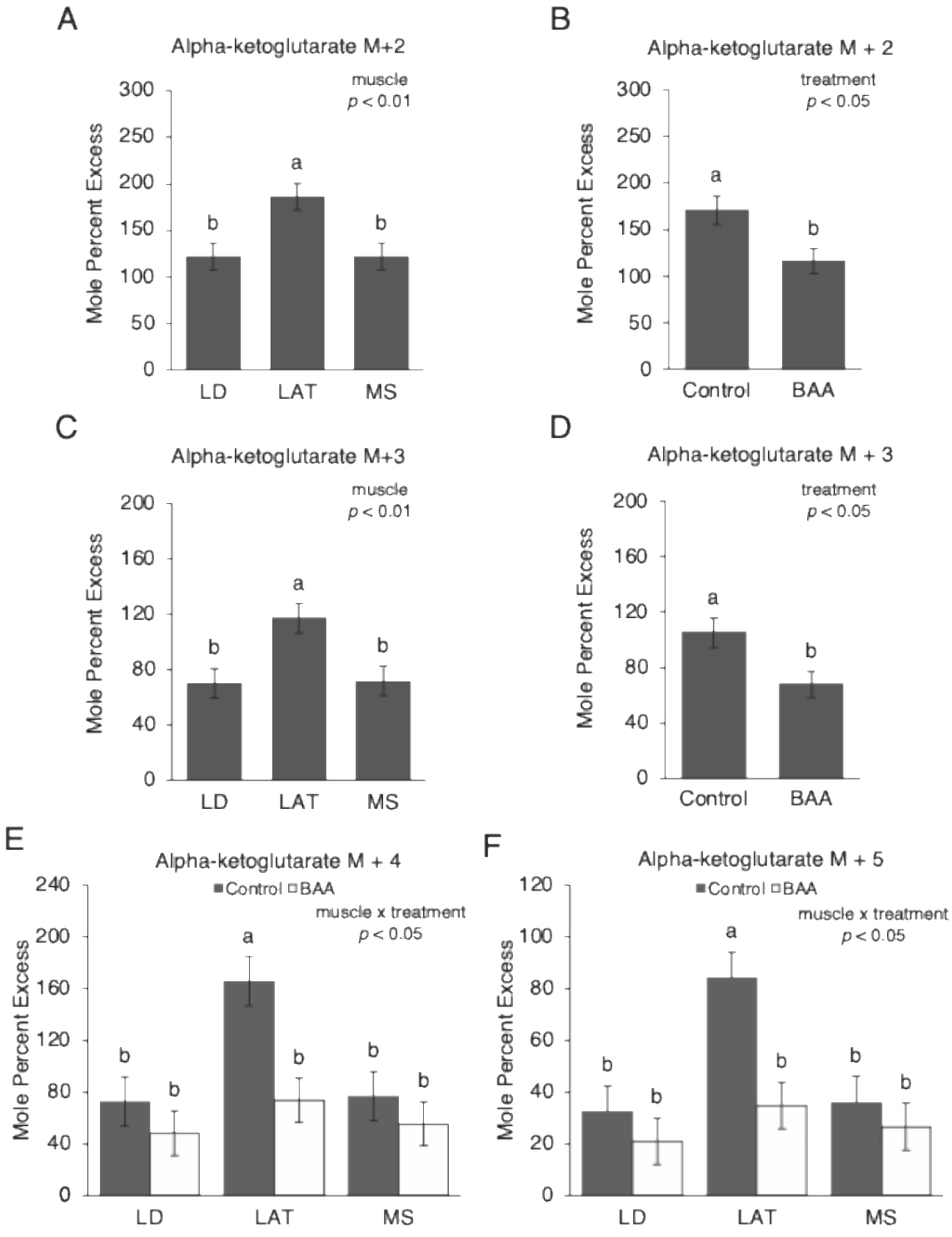

Figure 2.9. Enrichments of alpha-ketoglutarate from [$^{13}C_3$]-pyruvate in isolated mitochondria. Enrichment of **(A-B)** M + 2, **(C-D)** M + 3, **(E)** M + 4, and **(F)** M + 5 alpha-ketoglutarate in LD, LAT and MS mitochondria isolated from control and BAA pigs. Data are shown as means ± SE. Ten BAA barrows (n = 10) and eight control barrows (n = 8) per group. Means lacking a common letter (a, b) differ ($p < 0.05$).

4. Discussion

In this study, feeding ractopamine hydrochloride for 2 wks at 9 g/ton did not result in the expected phenotypical response reported by many others. For example, Gonzalez et al. (2007) found an increase in the CSA of type I fibers in cattle fed 15 g/ton ractopamine for 92 d. Watkins et al. (1990) reported an increase in LEA and decrease in fat depth in pigs fed 2.3 g/ton and 4.5 g/ton BAA for 45 d, respectively. Similarly, Carr et al. (2005) and Panisson et al. (2020) showed an increase in LEA in pigs fed BAA at 9 and 18 g/ton for 25 to 41 d and 10 g/ton for 26 d, respectively. The lack of phenotypic differences in our data could be attributed to the amount and length the BAA was fed. Concentration of ractopamine hydrochloride was selected to comply with the FDA's maximum legal limit, which is 9 g/ton. In addition, commercial swine undergo continuous genetic selection for superior performance, resulting in enhanced genetics with each generation. Given we used the same genetics used in commercial production, it is reasonable to assume a greater concentration or longer duration of BAA feeding is required to alter muscle and fat deposition. While we did not observe phenotypic differences, our main objective of feeding ractopamine hydrochloride was to define the metabolic response of skeletal muscle after BAA feeding. Therefore, we evaluated MyHC protein abundance, relevant metabolic enzymes, metabolite concentration, and mitochondrial pyruvate utilization in muscles with inherently different metabolic profiles between treatment groups.

Evaluating MyHC isoforms is a traditional approach to classify the metabolic profile of skeletal muscles. To begin to investigate if BAA feeding induced a metabolic shift, protein abundance of MyHC isoforms were measured. There were no treatment differences in MyHC isoforms. However, a shift in MyHC gene expression has been reported in several studies that fed BAA to finishing pigs (Depreux et al., 2002; Gunawan et al., 2007; Almeida et al., 2015; Gunawan

et al., 2020). This discrepancy between our data and previous reports may be partially attributed to feeding conditions or the use of gene expression to measure MyHC isoforms rather than protein abundance. Further, the long protein turnover rate of myosin may mask underlying changes in metabolism studies. Indeed, its half-life of 14.5 days is longer than our duration of feeding (Rolfs et al., 2021). Conversely, there were differences in MyHC composition between muscles as expected. To further investigate if BAA muscle stimulates a change in metabolism, we assessed several metabolic enzymes that are associated with classifying skeletal muscle metabolism.

Abundance of metabolic enzymes provide insight into the profile of skeletal muscle metabolism. There were no differences PFK activity or LDHα protein abundance between treatments. This is similar to results reported by Gunawan et al. (2007), who reported no difference in LDHα expression between 1 and 4 wks of feeding 18 g/ton ractopamine. In addition, we assessed muscles with different types of metabolism to determine if they responded differently to BAA supplementation. Further, while highly oxidative and highly glycolytic muscles have been well characterized, mixed muscles have a more complex metabolic profile. For example, Rimmer et al. (2024) reported LAT and MS muscles were similar in PC abundance, but LD and LAT muscles were similar in LDHα abundance.

Evaluating changes in enzymes associated with the TCA cycle allows for a deeper understanding of metabolic differences within skeletal muscle. For example, oxidative fibers exhibit a high abundance and activity of SDHα. Therefore, prior to metabolite analysis, we evaluated the abundance of PC and SDHα. A difference in PC abundance could be indicative that pyruvate is being utilized differently in muscle. Therefore, we wanted to further investigate the differences in metabolite utilization.

To determine if BAA feeding alters glucose utilization, we evaluated the concentration of glucose, G6P, and lactate. In all muscles evaluated, glucose and G6P concentration decreased due to treatment. However, there were no treatment differences in lactate levels, which corresponds to the lack of differences in LDHα abundance. These data indicate ractopamine hydrochloride stimulates muscle to utilize glucose differently than control muscles. BAA supplemented muscles could be prioritizing the PPP or serine biosynthesis pathway, which branch off from glycolysis. Additionally, lactate production in these muscles could be prioritized. There were muscle differences in glucose, G6P, and lactate concentrations as expected. Glucose and G6P concentration were lowest in the ST and MS and highest in the LD. Lactate concentration was highest in the LAT, second highest in the LD, third highest in the ST, and lowest in the MS. Interestingly, concentration of these glycolytic intermediates in ST muscles more closely resemble that of the MS. Conversely, ST muscles resembled glycolytic LD muscle in its large CSA, MyHC composition, high PFK activity, and high LDHα abundance. These data support the notion that mixed muscles may utilize different aspects of the major metabolic pathways to accommodate their energy requirements. However, the heterogeneity of the ST presents a technical challenge as its fiber composition varies across the muscle. For example, Graziotti et al. (2011) found that the medial portion of the ST presented as more oxidative in its composition.

Differences in glucose and G6P as well as PC abundance in BAA muscle questions if pyruvate utilization is altered within BAA mitochondria. Pyruvate can be shuttled into the TCA cycle through PC or PDH. Entry into the cycle by PDH can be considered inefficient in regard to livestock production efficiency due to its loss of a carbon dioxide molecule during the conversion of pyruvate to acetyl-CoA. Alternatively, entry through PC has the capacity to preserve carbon molecules by consuming one bicarbonate and one ATP molecule to produce oxaloacetate from

pyruvate. Indeed, PC is upregulated in the LD of pigs classified with superior feed efficiency (Fu et al., 2017). To assess pyruvate utilization in BAA mitochondria, we implemented an *in vitro* tracing strategy using isolated mitochondria. Isotopomer tracing can aid in understanding the entry of pyruvate into the TCA cycle as well as reveal changes in overall utilization of the metabolite. For example, an increase in citrate M + 2 is attributed to an increase in PDH-mediated entry of pyruvate into the TCA cycle (Gravel et al., 2014; Duan et al., 2022). Alternatively, when labeled pyruvate enters through PC and is converted to oxaloacetate with the addition of a bicarbonate molecule, oxaloacetate M + 3 can be formed (Gravel et al., 2014). Similarly, citrate M + 3 could indicate PC-mediated entry (Figure 6). However, it is important to acknowledge intermediates can be shuttled in and out of the TCA cycle depending on cellular demands, and these are theoretical labeling patterns. Regardless, changes in isotopomer enrichment depict alterations in the utilization of a given metabolite.

Enrichment of citrate M + 2, M + 3, and M + 4 increased in control LAT compared to all other mitochondria, which suggests an increase in pyruvate entering the TCA cycle regardless of entry point in control LAT mitochondria. Further, α-ketoglutarate M + 2 and M + 3 increased in all control mitochondria compared to BAA mitochondria, and enrichment of these isotopomers was highest in LAT mitochondria regardless of treatment. Enrichment of α-ketoglutarate M + 4 and M + 5 increased in LAT mitochondria compared to all other mitochondria. Taken together, these findings suggest BAA alters pyruvate entry and utilization in LAT mitochondria and diminishes M + 2 and M + 3 α-ketoglutarate enrichment in LD and MS mitochondria. This notion is supported by LAT muscles exhibiting an increase in PC abundance compared to all other muscles while it is the lowest in BAA muscles compared to control muscles. Due to technical limitations, we were unable to assess BAA mediated changes in PDH. On the other hand, OAA M

+ 2 increased in BAA LD and LAT mitochondria compared to all MS mitochondria. Additionally, OAA M + 2 increased in BAA LAT compared to control LAT mitochondria. These data question if BAA supplementation utilizes glucose derived intermediates in cataplerotic reactions, which could be supporting numerous physiological processes rather than undergoing complete oxidation for energy production. However, additional research is needed to elucidate these processes. While the intricacies of anaplerosis and cataplerosis in the TCA cycle pose a challenge to defining the mechanisms that drive altered mitochondrial glucose utilization, these data suggest supplementation of BAA in swine diets cause changes in pyruvate and metabolite usage in mitochondria with different metabolic profiles.

5. Conclusion

While there are multiple methods used to define skeletal muscle metabolism, our findings demonstrate the intricacies of evaluating metabolic shifts in skeletal muscle. We did not observe the expected phenotypic response of BAA feeding, which may be attributed to duration and dosage of ractopamine hydrochloride supplementation. Further, BAA supplementation herein did not stimulate changes in MyHC isoforms or most metabolic enzymes evaluated. However, we provide evidence that glucose utilization is altered in BAA muscle, which may occur in a muscle specific manner. Therefore, when investigating metabolic shifts in finishing pigs, subtle changes in metabolite utilization can be detected. Findings highlight the importance of a broad investigation into metabolism that incorporates multiple approaches. Although it is clear glucose utilization is altered in BAA muscle, additional research is needed to define this mechanism of action to translate findings to the industry.

References

Almeida, V. V., A. J. C. Nuñez, A. P. Schinckel, M. G. Ward, C. Andrade, M. Sbardella, B. Berenchtein, L. L. Coutinho, and V. S. Miyada. 2015. Gene expression of beta-adrenergic receptors and myosin heavy chain isoforms induced by ractopamine feeding duration in pigs not carrying the ryanodine receptor mutation. Livestock Science 172:91-95. doi:10.1016/j.livsci.2014.12.007

Carr, S. N., D. J. Ivers, D. B. Anderson, D. J. Jones, D. H. Mowrey, M. B. England, J. Killefer, P. J. Rincker, and F. K. McKeith. 2005. The effects of ractopamine hydrochloride on lean carcass yields and pork quality characteristics. Journal of Animal Science 83:2886-2893. doi:10.2527/2005.83122886x

Depreux, F. F., A. L. Grant, D. B. Anderson, and D. E. Gerrard. 2002. Paylean alters myosin heavy chain isoform content in pig muscle. J Anim Sci 80:1888-1894. doi:10.2527/2002.8071888x

Deshpande, O. A., and S. S. Mohiuddin. 2024. Biochemistry, Oxidative Phosphorylation. StatPearls, Treasure Island (FL).

Dohlman, E., J. Hansen, and D. Boussios. 2022. USDA Agricultural Projections to 2031.

Duan, L., D. E. Cooper, G. Scheidemantle, J. W. Locasale, D. G. Kirsch, and X. Liu. 2022. (13)C tracer analysis suggests extensive recycling of endogenous CO(2) in vivo. Cancer Metab 10:11. doi:10.1186/s40170-022-00287-8

El-Kadi, S. W., R. L. t. Baldwin, K. R. McLeod, N. E. Sunny, and B. J. Bequette. 2009. Glutamate is the major anaplerotic substrate in the tricarboxylic acid cycle of isolated rumen epithelial and duodenal mucosal cells from beef cattle. J Nutr 139:869-875. doi:10.3945/jn.108.103226

Essen, B., E. Jansson, J. Henriksson, A. W. Taylor, and B. Saltin. 1975. Metabolic characteristics of fibre types in human skeletal muscle. Acta Physiol Scand 95:153-165. doi:10.1111/j.1748-1716.1975.tb10038.x

Fu, L., Y. Xu, Y. Hou, X. Qi, L. Zhou, H. Liu, Y. Luan, L. Jing, Y. Miao, S. Zhao, H. Liu, and X. Li. 2017. Proteomic analysis indicates that mitochondrial energy metabolism in skeletal muscle tissue is negatively correlated with feed efficiency in pigs. Sci Rep 7:45291. doi:10.1038/srep45291

Gonzalez, J. M., J. N. Carter, D. D. Johnson, S. E. Ouellette, and S. E. Johnson. 2007. Effect of ractopamine-hydrochloride and trenbolone acetate on longissimus muscle fiber area, diameter, and satellite cell numbers in cull beef cows. J Anim Sci 85:1893-1901. doi:10.2527/jas.2006-624

Gravel, S. P., S. Andrzejewski, D. Avizonis, and J. St-Pierre. 2014. Stable isotope tracer analysis in isolated mitochondria from mammalian systems. Metabolites 4:166-183. doi:10.3390/metabo4020166

Graziotti, G. H., J. M. R. Men챕ndez, C. M. R챠os, M. E. Cossu, A. Bosco, N. O. Affricano, A. P. Ceschel, S. Mois찼, and L. Basso. 2011. Relationship between Myosin Isoforms and Meat Quality Traits in Pig Semitendinosus Neuromuscular Compartments. Asian-Australas J Anim Sci 24:125-129. doi:10.5713/ajas.2011.10237

Gunawan, A. M., B. T. Richert, A. P. Schinckel, A. L. Grant, and D. E. Gerrard. 2007. Ractopamine induces differential gene expression in porcine skeletal muscles. J Anim Sci 85:2115-2124. doi:10.2527/jas.2006-540

Gunawan, A. M., C. N. Yen, B. T. Richert, A. P. Schinckel, A. L. Grant, and D. E. Gerrard. 2020. Ractopamine-induced fiber type-specific gene expression in porcine skeletal muscles is independent of growth. J Anim Sci 98. doi:10.1093/jas/skaa341

Hammelman, J. E., B. C. Bowker, A. L. Grant, J. C. Forrest, A. P. Schinckel, and D. E. Gerrard. 2003. Early postmortem electrical stimulation simulates PSE pork development. Meat Sci 63:69-77. doi:10.1016/s0309-1740(02)00057-8

Matarneh, S. K., C. N. Yen, J. Bodmer, S. W. El-Kadi, and D. E. Gerrard. 2021. Mitochondria influence glycolytic and tricarboxylic acid cycle metabolism under postmortem simulating conditions. Meat Sci 172:108316. doi:10.1016/j.meatsci.2020.108316

Panisson, J. C., A. Maiorka, S. G. Oliveira, A. Saraiva, M. S. Duarte, K. F. Silva, E. V. Santos, R. L. S. Tolentino, I. M. G. Lopes, L. L. M. Guedes, and B. A. N. Silva. 2020. Effect of ractopamine and conjugated linoleic acid on performance of late finishing pigs. Animal Frontiers 14:277-284. doi:10.1017/S1751731119001708

Peter, J. B., R. J. Barnard, V. R. Edgerton, C. A. Gillespie, and K. E. Stempel. 1972. Metabolic profiles of three fiber types of skeletal muscle in guinea pigs and rabbits. Biochemistry 11:2627-2633. doi:10.1021/bi00764a013

Pette, D., and R. S. Staron. 2000. Myosin isoforms, muscle fiber types, and transitions. Microsc Res Tech 50:500-509. doi:10.1002/1097-0029(20000915)50:6<500::AID-JEMT7>3.0.CO;2-7

Rimmer, L. A., E. R. Geisbrecht, M. D. Chao, T. G. O'Quinn, J. C. Woodworth, and M. D. Zumbaugh. 2024. Skeletal Muscle Metabolism Is Dynamic during Porcine Postnatal Growth. Metabolites 14:357.

Rolfs, Z., B. L. Frey, X. Shi, Y. Kawai, L. M. Smith, and N. V. Welham. 2021. An atlas of protein turnover rates in mouse tissues. Nat Commun 12:6778. doi:10.1038/s41467-021-26842-3

Tokach, M. D., B. D. Goodband, and T. G. O'Quinn. 2016. Performance-enhancing technologies in swine production. Animal Frontiers 6:15-21. doi:10.2527/af.2016-0039

Watkins, L. E., D. J. Jones, D. H. Mowrey, D. B. Anderson, and E. L. Veenhuizen. 1990. The effect of various levels of ractopamine hydrochloride on the performance and carcass characteristics of finishing swine. J Anim Sci 68:3588-3595. doi:10.2527/1990.68113588x